ECM STIFFNESS REGULATES THE MYOFIBROBLASTIC ACTIVATION AND CONTRACTILTIY OF CULTURED PRIMARY CORNEAL KERATOCYTES

by

Daniel Paul Maruri

APPROVED BY SUPERVISORY COMMITTEE:

Victor Varner, Chair

David Schmidtke

Matthew Petroll

For Nany.

ECM STIFFNESS REGULATES THE MYOFIBROBLASTIC ACTIVATION AND CONTRACTILTIY OF CULTURED PRIMARY CORNEAL KERATOCYTES

by

Daniel Paul Maruri, BS

THESIS

Presented to the Faculty of

The University of Texas at Dallas

in Partial Fulfillment

of the Requirements

for the Degree of

MASTER OF SCIENCE IN

BIOMEDICAL ENGINEERING

THE UNIVERSITY OF TEXAS AT DALLAS

May 2019

ACKNOWLEDGMENTS

I would like to thank Dr. David Schmidtke, Dr. Matthew Petroll, and Dr. Victor Varner for serving on my committee. I would like to express my deepest gratitude to Dr. Varner, I could not have accomplished what I have over the past 2 years without his outstanding encouragement, advice, and guidance. To everyone that attended weekly lab meetings at UT Southwestern, namely Dr. Schmidtke, Dr. Petroll, Dr. Varner, Dr. Miguel Mendoza, Kevin Lam, Pouriska Kivanany, and Kyle Gross, thank you all for the tremendous advice and insight. I would like to express my appreciation to Dr. Petroll and Dr. Schmidtke for welcoming me into their lab and allowing me to borrow/access equipment and lab space for my experiments. I want to send my thanks to everyone in the Varner Lab at UT Dallas, it has been a pleasure working with all of you over the past years. Your input and encouragement was greatly appreciated. I would lastly like to thank all my friends and family that patiently listened to my spiels about keratocytes and wound healing over the past years. Specifically, I want to acknowledge my mother, father, and brother. My father, Eduardo Maruri, for instilling in me the qualities and passion to succeed as an engineer. My mother, Michele Maruri, for always picking me up and pushing me forward when life became tough. My brother, Eddie Maruri, for being an inspiration, and challenging me to always be better. Lastly, I want to recognize my late grandmother, Adrianna “Nany” Maruri, not a day goes by where I don’t think of her words inspiring me towards my goals.

January 2019

ECM STIFFNESS REGULATES THE MYOFIBROBLASTIC ACTIVATION AND CONTRACTILTIY OF CULTURED PRIMARY CORNEAL KERATOCYTES

Daniel Paul Maruri, MS
The University of Texas at Dallas, 2019

Supervising Professor: Victor Varner, PhD

Following surgery or traumatic injury, corneal wound healing can cause a scarring response that impairs ocular function. This fibrosis is caused, in part, by the activation of corneal keratocytes from a native quiescent state to an activated myofibroblastic state. Signaling pathways downstream of transforming growth factor beta 1 (TGF-β1) have been shown to be key regulators of this transformation. During wound healing, the activated corneal keratocytes begin to secrete fibrotic extracellular matrix (ECM) proteins and to exert contractile forces to close the wound. These behaviors, however, can disrupt the organization of the ECM in the corneal stroma and reduce the transparency of the tissue. Previous studies have suggested that biophysical cues can modulate keratocyte behavior, but it remains unclear how the activation and contractility of corneal keratocytes is regulated by changes in ECM stiffness. Here, to better understand how ECM stiffness interacts with TGF-β1 signaling to regulate myofibroblastic activation, we cultured primary rabbit corneal keratocytes on compliant, collagen-coated substrata of varying stiffness in either the presence or absence of TGF-β1. Polyacrylamide hydrogels were fabricated on glass coverslips and functionalized to perform two-dimensional (2D) cell culture and traction force microscopy (TFM). The gels were then plated with primary corneal keratocytes, isolated from rabbit eyeballs, as described previously, and cultured at 37°C in either serum-free media or media

containing exogenous TGF-β1. Time-lapse fluorescence microscopy was used to assess changes in cellular morphology, as well as to track motion of the fluorescent microspheres embedded within the gel. The tracked bead motion was then used to estimate the traction stresses exerted by the cultured keratocytes under different experimental conditions. In other experiments, cells were fixed after 5 days of culture and stained for molecular markers of either contractility or myofibroblastic transformation. Treatment with TGF-β1 elicited distinct cellular phenotypes when keratocytes were cultured on gels of different stiffness. Keratocytes cultured on either 10 kPa (stiff) gels or glass coverslips had broad cellular processes, formed abundant stress fibers, exhibited elevated levels of alpha smooth muscle actin immunofluorescence, and exerted large traction forces. Cells cultured on 1 kPa (soft) gels, however, formed few stress fibers, exerted small traction forces, and retained an elongated morphology, indicative of a more quiescent phenotype. Confocal images of phosphorylated-myosin light chain (pMLC) immunofluorescence, moreover, revealed stiffness-dependent variations in the spatial distributions of sub-cellular contractility. Our computed traction force maps correlated strongly with the observed spatial patterns of pMLC immunofluorescence. Taken together, these data suggest that changes in ECM stiffness, often associated with tissue fibrosis, can modulate the contractility and differentiation of corneal keratocytes during wound healing.

TABLE OF CONTENTS

LIST OF FIGURES

APPENDIX B FIGURES

LIST OF TABLES

APPENDIX A TABLES

CHAPTER 1: INTRODUCTION

1.1 BACKGROUND

It is estimated that more than 40% of the U.S. population develop ocular impairments that require the aid of glasses or contacts[1]. Myopia, or nearsightedness, is one of the most prevalent disorders that causes visual deficiency, and it is estimated that nearly 30% of the U.S. population is currently suffering with the condition[2,3]. Although the use of glasses or contact lens is sufficient for some patients, others require refractive surgery to restore their vision. As light enters the eye, it first passes through the thin layer of tissue at the front of the eye called the cornea. As light passes though the cornea it will bend, or refract, inward towards the back of the eye to the retina. When the cornea is abnormally shaped, light is refracted improperly through the eye and ocular function diminishes. Thus, by remodeling the cornea through refractive surgeries such as laser-assisted in situ keratomileusis (LASIK) and photorefractive keratectomy (PRK), chronic visual impairments, such as myopia, hyperopia and astigmatism can be reversed.

Briefly, the process of PRK involves local removal of the epithelial layer of cells from the cornea and using an excimer laser to sculpt the curvature of the cornea to more precisely refract light to the retina[5] (Figure. 1, left). An excimer laser that uses short wavelength ultraviolet light to vaporize and mold the cornea. As a first generation surgery, PRK provided for sustained visual recovery but could result, in some cases, hazy vision and vision regression[49]. LASIK was thus developed as an alternative to PRK. LASIK also molds the cornel stroma but, access to the stroma is not achieved by ablating the corneal epithelium. Rather, a flap is made in the epithelium, which is peeled back to reveal the stroma and closed at the end of the surgery[5] (Figure. 1, middle). By preserving the epithelium, the recovery time for the patient could be lessened and the pain reduced.

Similar to PRK, however, LASIK has its own disadvantages. Patients that have undergone LASIK surgery have experienced corneal hazing, dry eyes, and flap complications[49].

Although LASIK and PRK have been used for decades to provide visual correction, a new technique was recently approved by the FDA in 2016 and has been used for to treat patients with myopia[50]. The procedure, termed Small Incision Lenticule Extraction (SMILE), uses a femtosecond laser to excise a lens-shaped tissue, or lenticule, within the cornea, which is removed manually via a small incision in the cornea (Fig. 1, right). Although SMILE is a novel technique that improves some of the negative effects of LASIK, it can only be utilized if the patient is nearsighted.

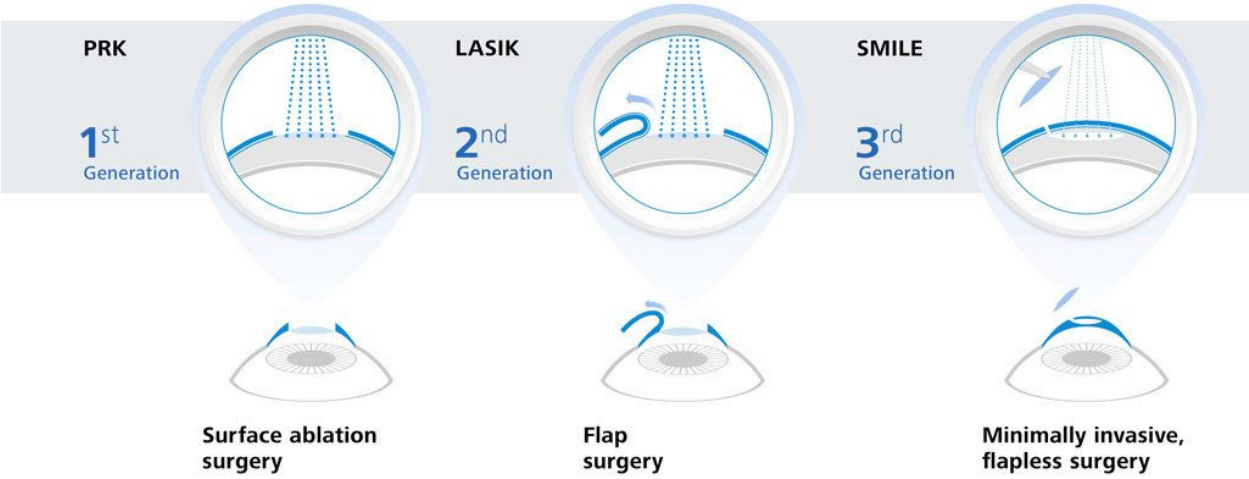

Figure 1. Schematic showing the differences between PRK, LASIK and SMILE. In PRK procedures the epithelial layer is removed in order to access the stroma. In LASIK and PRK, a flap or small incision is created to access the stromal layer. Retrieved from LaserVue Eye Center's[11] website.

Although all three surgeries can help be used restore a patient's vision, they all will involve some range of damage to the corneal stroma as it is laser molded to a specific curvature. As discussed in detail below, the corneal stroma plays an important role in the cornea's ability to bend

light towards the retina. If damaged, this can cause side effects such as corneal hazing, "halos" around objects, and blurry vision. Many of these side effects are caused by the changes in behaviors of the cells that reside within the stroma, the corneal keratocytes.

The purpose of this thesis is to address the role that mechanical stiffness plays when primary corneal keratocytes are subjected to exogenous growth factors that are characteristic of a wound healing response. By plating normal rabbit keratocytes on to flexible polyacrylamide gels in the presence, or absence, of growth factors typical of a wound healing response, we can observe changes in cell phenotypes. Results from this study could be potentially used in devising new technologies focused towards improving wound healing in the cornea and other organs of the body.

1.2 CORNEAL ANATOMY

The cornea is a transparent soft tissue located at the anterior of the eye. It acts as both a mechanical barrier protecting the inner eye and provides approximately $^2/_3$ of the refractive power needed to bend light toward the retina at the back of the eye[7]. The structure of the cornea consists of five distinct layers, from anterior to posterior: the epithelium, Bowman's layer, stroma, Descemet's layer, and endothelium (Fig. 2). The corneal epithelium is located at the outmost anterior of the cornea. It's comprised of a single layer of basal cells overlaying 4-5 layers of tightly packed squamous epithelial cells. This creates an efficient barrier to against pathogens and fluid loss from the inner eye[7,8]. Beneath the epithelium is Bowman's membrane. It consists of a basement membrane containing type I collagen, and acts as a divider between the stroma and epithelium. This membrane serves an important role in preventing any transport of cytokines between the epithelial and stromal tissue compartments[8]. Underneath Bowman's membrane, the collagen-rich corneal stroma spans nearly 90% of the total corneal thickness[23]. The stroma plays a

crucial role in the refractive power needed by the cornea to guide light to the retina. Below the stroma lies the Descemet's layer; which, similar to the basement membrane, is a thin layer of collagen that acts as a divider between the stromal and the endothelial compartments. Ultimately, the endothelium marks the most posterior layer of the cornea. The endothelium is single layer of squamous cells that has the main function of "pumping" out fluid in the corneal stroma in order to avoid edema[13] (Fig 2).

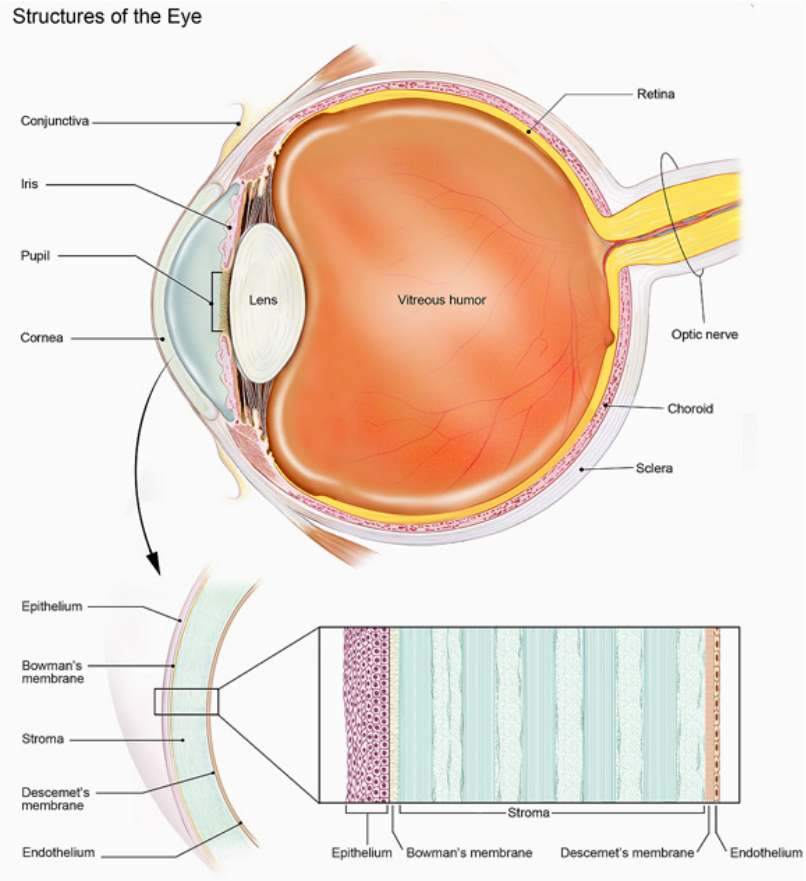

Figure 2. Anatomical structure of the eye and cornea[9]. Looking at the cornea, from anterior to posterior, the 5 main layers include the epithelium, Bowman's membrane, stroma, Descemet's membrane, and endothelium. Image credit to the National Eye Institute and National Institutes of Health[9].

Although each of these layers is important in maintaining ocular function, key among them is the corneal stroma. One of the main features of the stroma is the precise organization of its ECM microstructure. The microstructure of the stroma is characterized mainly by fibrils of type I and V collagen[22,23,18], which are distinctively aligned in parallel arrays. Layers of these collagen lamellae are orthogonally stacked on top of one another, which allows for the free passage of light through the tissue, thus giving rise to its unique transparency[13] (Fig. 3). Corneal keratocytes are natively quiescent fibroblastic cells which reside between the sheets of collagen lamellae of the corneal stroma[17,18] (Fig. 3). Keratocytes are responsible for secreting ECM proteins to maintain and develop normal corneal structure[17,18]. However, upon injury to the cornea these cells are capable of transforming into a repair phenotype in order to reestablish structural integrity to the stroma. As mentioned above, damage to the stroma can occur as a result of traumatic injury or as a side effect of refractive surgery. The next section will explore the healing process and the role of the keratocyte in closing the wound.

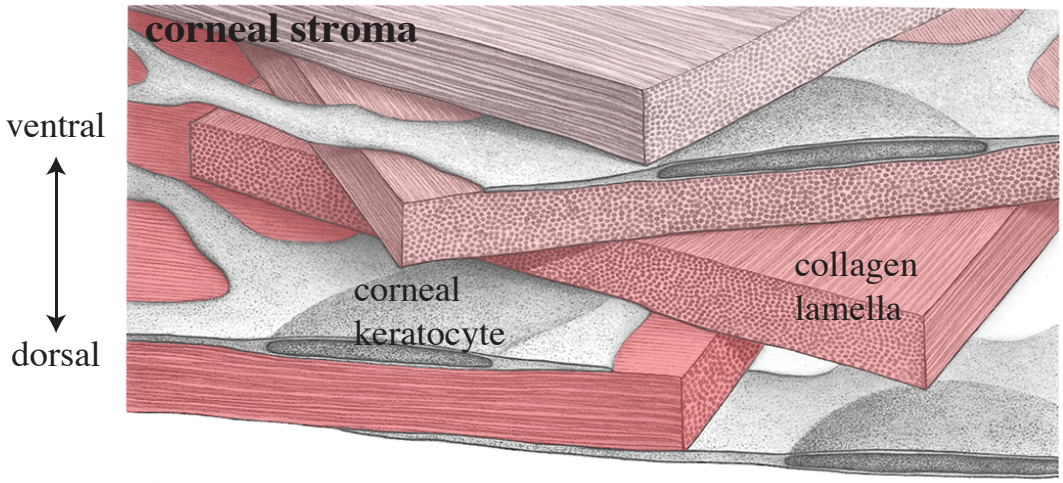

Figure 3. Illustration of the microstructure of the corneal stroma. Sheets of collagen I lamella are precisely aligned in stacks to make up the thickness of the stroma. Within the layers of collagen lay quiescent corneal keratocytes, which maintain the ECM of the corneal stroma. Adapted from Hogan et al (1971)

1.3 INJURY AND WOUND HEALING RESPONSE

Being at the foremost anterior of the eye, the cornea is constantly at risk at becoming injured during normal day activity. The epithelial layer of cells is acting as a first line of defense against bacteria and any foreign bodies that could potential cause harm to the cornea and inner eye. However, if damage goes beyond Bowman's layer and into the stroma of the cornea, repair of the stromal ECM will be carried out by the keratocyte. As discussed previously, refractive surgeries require the permanent or temporary removal of the epithelium and a reshaping of the corneal stroma[4,6,22]. Damage past the Bowman's layer, and consequently the corneal stroma, causes a release of epithelial-derived and stromal-derived growth factors, cytokines and proteinases into both the stroma and the epithelium[8,19]. This crosstalk of exogenous biomolecules between the two layers initiates the wound healing response of cells in each compartment. For this study, we will focus solely on processes in the stroma.

Epithelial growth factors and cytokines diffuse into the corneal stroma after an injury occurs[19]. The first response by keratocytes directly below the injury site is an apoptotic reaction caused by the release of interleukin-1 (IL-1)[19,20]. Other cells in the area around the wound site will become activated by several growth factors: transforming growth factor beta 1 (TGF-β1)[24], platelet-derived growth factor-BB (PDGF-BB)[25], fibroblast growth factor 2 (FGF-2)[26,27], and epidermal growth factor (EGF). Key among these growth factors is TGF-β1. Normally quiescent keratocytes in the stroma will become activated by TGF-β1, resulting in a transformation into a myofibroblastic phenotype. Cells are activated by TGF-β1 will become contractile and start to secrete new ECM proteins to close the wound[21,29] (Fig. 4).

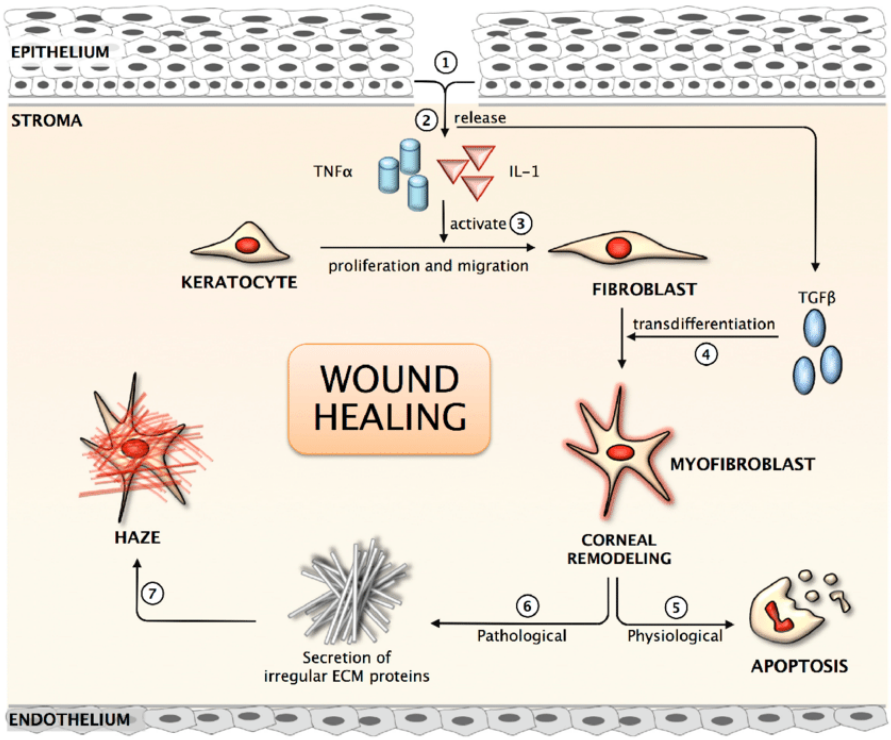

Figure 4. Generalized schematic of wound healing in the cornea in response to TGF-β1. Upon injury beyond the epithelium and Bowman's layer, epithelial growth factor TGF-β1 will enter the stroma and initiate a myofibroblastic transformation by corneal keratocytes. Adapted from Chaurasia et al (2015).

Although this transformation is beneficial in the healing of the cornea, there are a couple of significant disadvantages. First, as the cell contracts it will pull hard on the surround collagen lamellae of the cornea stroma, this can cause disorder within the highly-aligned ECM matrix[30]. Moreover, the fibrotic response will result in the release new, disorganized ECM proteins. When these behaviors are coupled together, changes in cornea shape can occur due to the addition of new tissue and rearrangement of mechanical tension within the stroma[35]. As pointed out earlier, the spatial patterning and orientation of the collagen filaments is essential for the passive transition of light through the cornea. Disorganization of the matrix increases the amount of light scattering within the stroma which ultimately leads to a reduction in transparency[31,32,33]. In addition, an

increase in stiffness characteristically accompanies any fibrotic response due to injury[51]. It has been shown that the change in stiffness of the ECM is important in regulating the behaviors of cells[52]. However, it is still unclear how stiffness effects the behavior of the corneal keratocyte and which intracellular pathways are driving phenotypic changes.

1.4 THE ROLE OF STIFFNESS AND MECHANOTRANSDUCTION

As described, once the cells become activated and transform to a myofibroblastic state they will start to repair the wound site by excreting new ECM and contracting to close the injury. This fibrotic response will create granulated, scar tissue in the wound area. In human corneal tissue, the elastic modulus is on the order of 22 kPa[79], but in the presence of scar tissue is an increase in stiffness to about 71 kPa[36]. This alteration of mechanical stiffness has a considerable influence on the behavior of cells.

In our bodies, cells are constantly probing their environment, sensing both biophysical and biochemical stimuli that regulate their behaviors. Through the combination of mechanotransduction and mechanosensing, cells are able to actively respond to the rigidity of their environment. Mechanotransduction can best be defined by the process of translating mechanical information, gathered from mechanosensing, into biological responses. This is often mediated by signaling downstream of integrin receptors, or transmembrane proteins that form mechanical connections between the cell cytoskeleton and ECM[53]. When a cell exerts forces on the substrate to which it is attached, depending on the stiffness, this can trigger changes in intracellular components and cellular behaviors - cytoskeletal organization, cellular biochemical localization, contractility[54]. While many of the pathways involved in stiffness-sensing have been identified – YAP/TAZ, MRTFA, FAK [43,55,56,82]- it is still not clear how changes in ECM stiffness might

regulate the activation of corneal keratocytes.

One way to assess how modulating ECM stiffness alters cellular behavior is to observe intracellular changes. Zooming into the cell, one finds that much of what controls the cell is made possible through biochemical changes. For instance, receptors imbedded within the cell membrane are able to detect exogenesis ligands that, when bound to a receptor, trigger a cascading pathway within the cell. Pathways allow for a swift response to an external stimulus. When focusing on mechanotransduction, the GTPase proteins Rho, Rac, and Cdc42 pathways play significant roles in responding to the stiffness of the ECM and modulating cell morphology, focal adhesion formation and contractility. Activated Rho GTPase will initiate the formation of focal adhesions and stress fibers within the cell body[39]. The activation of Rho pathways is tightly knit with cytoskeletal contractility. As Rho pathways initiate, there will be an increase the phosphorylation of myosin motors, thus causing actomyosin to contract[40]. Contrary to Rho pathways, when the Rac pathway is activated by its GTPase receptor there is an increase in cell spreading and cell migration via treadmilling actin polymerization and smaller nascent focal adhesion formation[41,42].

Another important mediator of cellular function are transcriptional regulators. Specifically, one regulator protein pair that has gained a lot of attention in recent studies are yes-associated protein (YAP) and transcriptional coactivator with PDZ-binding motif (TAZ)[43]. YAP/TAZ will enter the nucleus and regulate gene transcription by interacting to binding domains in DNA which will result in a change in cell contractility, differentiation and proliferation[44,45,46]. When the hippo signaling is “off”, YAP/TAZ activity within the nucleus increases; conversely, when it is “on” activity decreases. But how does this relate to stiffness? When cells are plated onto a stiff substrate, they will bind and spread along the surface. Upon attachment, filamentous actin (F- actin) coupled

with myosin motors form contractile bundles within the cell. In the presence of contractile F-actin, hippo signaling will decrease and YAP/TAZ will localize within the nucleus. Contrarily, on soft substrates the hippo pathway will flip "on", thus causing YAP/TAZ to become localized in the cytoplasm of the cell where it will be digested by proteases. Overall, on stiff surfaces cells are characterized by strong contractile forces, differentiation of mesenchymal stem cells is directed towards an osteoblastic lineage, and proliferation increases. On the contrary, when placed on a soft substrate, YAP and TAZ are more likely to remain in the cytoplasm of the cell, and ultimately digested. Under this condition, cells are characterized by low contractile forces, mesenchymal stem cells differentiation is guided towards adipogenic lineages, and apoptosis is favored[57,58,59] (Fig. 5).

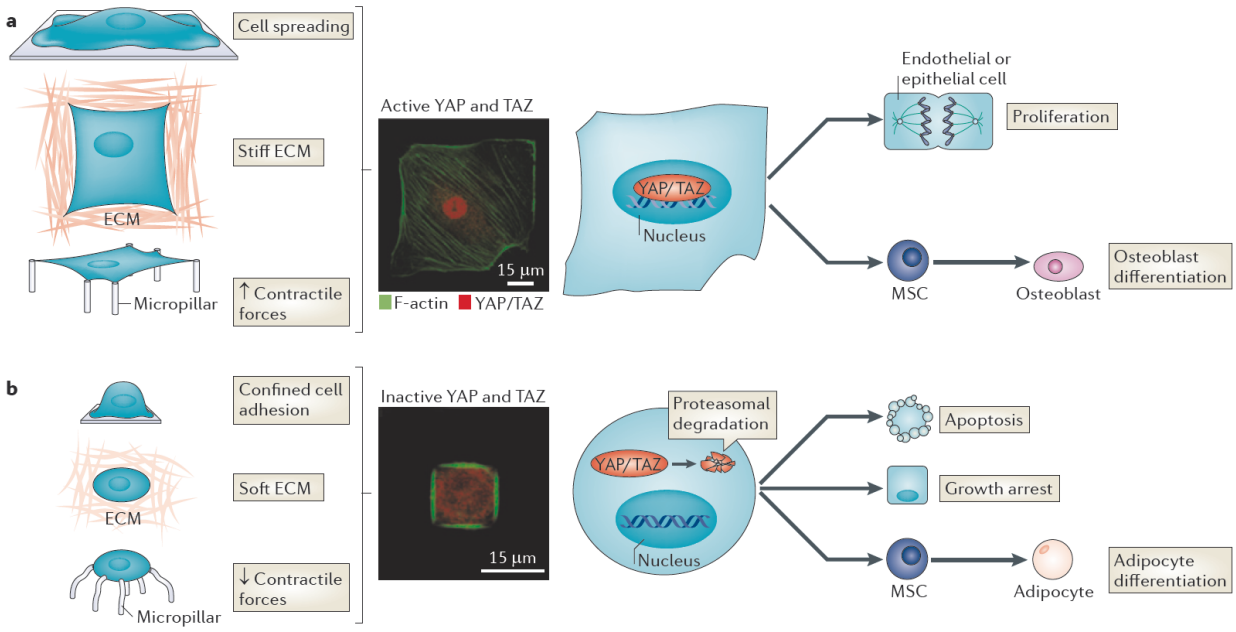

Figure 5. Schematic of YAP/TAZ localization as ECM stiffness, cell shape, and adhesion spacing are adjusted. Specifically addressing the effects of stiffness, on more compliant substrates the YAP/TAZ localization is localized to the cytoplasm where it will be digested by proteases. On stiffer substrates, YAP/TAZ localization transitions into the nucleus where it will bind to DNA. Image retrieved from Dupont et al[57] (2011).

Lastly, one other key factor in a cell's ability to sense its environment are focal adhesions formation and their role in applying contractile stresses. As integrins begin to cluster they will start to recruit talin proteins. With the addition of talin, clusters of integrins are able to connect to the cytoskeleton of the cell and form nascent focal adhesions. As actin filament polymerize at the focal adhesion spots, myosin II motors are simultaneously exerting contractile forces from the cell onto the ECM. Studies have shown that as the stiffness of the microenvironment is increased, there is also an increase in focal adhesion size and number. This is because as the stiffness increases, this enables the cell to exert higher traction forces, thus create more mature focal adhesions[47] (Fig. 6). As integrins cluster and form focal adhesions, this initiates the activation of focal adhesion kinase (FAK). FAK it then able to regulate the Rho[60,62] and Rac[61,62] pathways which, as discussed before, play large roles in modulate the cytoskeletal structure and contractility of cells.

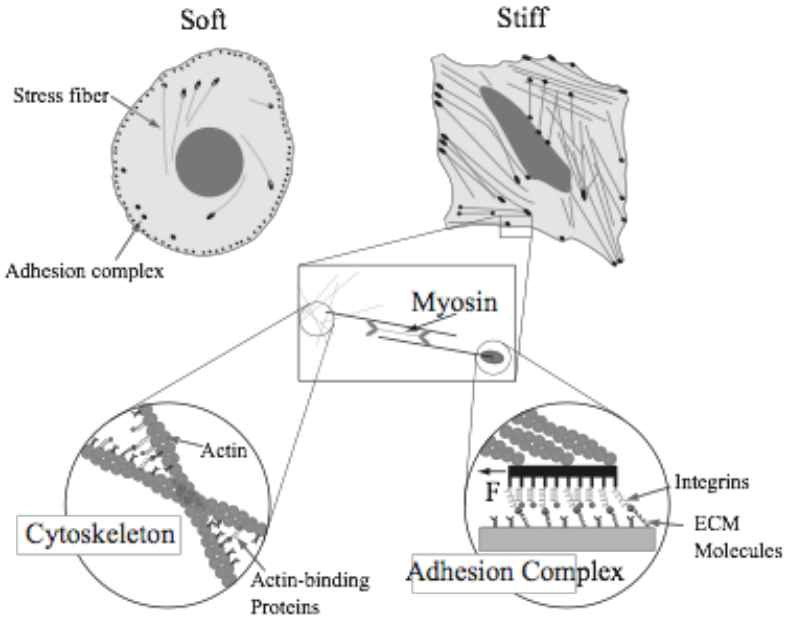

Figure 6. Schematic describing qualitative differences in focal adhesion formation and cytoskeletal structure on soft and stiff substrates. On stiff substrates, cells form more focal adhesions and stress fibers than those on more compliant substrates. Image adapted from Geiger et al (2009)[47].

It is apparent that stiffness plays a key role regulating cellular morphologies, contractility, and key intracellular molecular pathways. For these reasons, we hypothesize that keratocyte activation via TGF- β1 can be modulated by plating cells on flexible substrata.

1.5 POLYACRYLAMIDE HYDROGELS AND TFM

When cells are cultured in most experiments, they are usually plated on glass coverslips or tissue culture plastic. Both materials have an elastic modulus in range of gigapascals (GPa) which is considerably higher than most tissues found in the body. Hydrogels were first introduced by Wichterle and colleagues as they developed poly(2-hydroxyethyl methacrylate)-based hydrogels for use in contact lenses[63]. It wasn't until 1997 PAAM gels were first utilized by Robert Pelham and Yu-Li Wang to observe changes in cell motility and focal adhesion formation via modulating the stiffness if the substrate[64]. By lowering the elastic modulus of the substrata, they observed differences in cell morphology, motility and focal adhesion organization for epithelial and fibroblastic cell types[64]. Advantages of using PAAM as a cell culture platform are that it has (1) outstanding optical properties and can be fabricated very thin to allow for clear fluorescent imaging, (2) the ability to bind various ECM proteins to the surface of the gel, and (3) highly tunable elastic modulus. For these reasons, we have elected to use PAAM gels for our experiments.

By varying the ratios of crosslinkers to monomers, hydrogels can be fabricated at variable stiffness[65]. For our experiments, bis-acrylamide (2% w/v; Bis; Bio-Rad, Hercules, CA) crosslinkers and acrylamide (40% w/v;Am; Bio-Rad, Hercules, CA) monomers were used to create our PAAM hydrogels. To initiate polymerization, persulfate free-radicals in the system would then react with the acrylamide monomers to form free-radicals, these acrylamide free-radicals would then react with other inactivated acrylamide monomers to begin the polymerization chain

reaction[65] (Fig. 7). For this study, it was important to try to mimic the ECM stiffness of the corneal stroma both before and after a fibrotic response due to injury. It has been shown in rabbits that healthy stromal tissue has an elastic modulus of roughly 1.1 ± 0.6 kPa[10]; however, when normal, healthy tissue is replaced by scar tissue, there is a significant increase in elastic modulus. In these experiments, hydrogel stiffness was increase by one order of magnitude from 1 kPa to 10 kPa to replicate scar tissue formation.

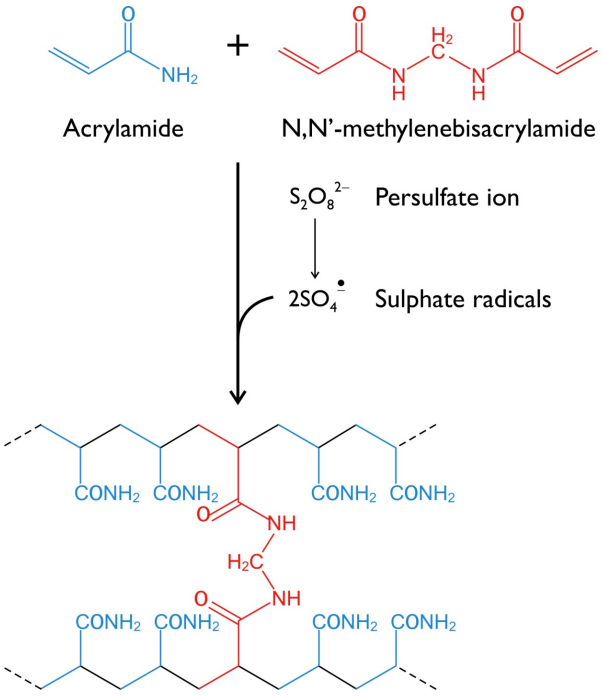

Figure 7. Schematic describing the chemistry of polyacrylamide gel fabrication[12]. Persulfate free-radicals in the system react with the acrylamide monomers to form free-radicals, these acrylamide free-radicals then react with other inactivated acrylamide monomers to form long chain polyacrylamide networks crosslinked by bis-acrylamide.

PAAM gels possess no binding sites for cells to attach, thus it is important to functionalize the gel for cell culture. This is accomplished by using the long arm crosslinker that has bifunctional properties. On one end of the molecule, there is a photoactivatable nitrophenyl azide group which,

when exposed to UV light, will covalently bind to PAAM gel. On the other end of the molecule is an amine-reactive N-hydroxysuccinimide (NHS) ester functional group which can bind to the primary amines in proteins to give the gel active binding sites for cell adhesion[65].

Polyacrylamide hydrogels have been able to be utilized in many different ways – 3D cell culture models[66], scaffolding[67], gel electrophoresis[68]. Recently, however, a lot of attention has been directed towards using PAAM gel in traction force microscopy (TFM). Seminal TFM experiments began in 1980 when Harris et al looked at how fish keratocytes migrated on flexible silicon substrata[69]. As the cell moved along the substrate, it would cause wrinkles in the material which could be used to qualitatively analyze the force being exerted by the cell. Today, polyacrylamide is extensively used because of its highly tunable mechanical properties, strong transparency, and ability to bind various ECM proteins[70]. By embedding fluorescent microspheres in the hydrogel, gel deformations can be visualized and, ultimately, traction forces can be precisely measured[71].

In this study, we will use a polyacrylamide system to modulate the stiffness of the microenvironment on which primary corneal keratocytes will be plated. TFM experiments utilizing fluorescent microspheres will be used to accurately quantify the traction stresses and forces being exerted by individual cells in the presence, or absence of exogenous growth factor on either soft or stiff PAAM gels. By changing the stiffness of the microenvironment, we hypothesize changes in morphology, activation, and contractility of the cultured corneal keratocytes.

CHAPTER 2: MATERIALS AND METHODS

In this study, a hydrogel-based system was used to create compliant substrata for 2D cell culture. PAAM is a well-suited material for this purpose, since it is optically transparent, can be functionalized with different ECM proteins, and has linear elastic mechanical properties with a tunable elastic modulus[64]. In addition, the use of functionalized PAAM allows for ECM composition to be decoupled from the mechanical properties of the gel. This chapter describes the methods employed to (i) fabricate PAAM gels of different stiffness, (ii) functionalize these gels with type I collagen, and (iii) make use of these gels as compliant substrata for 2D cell culture. We also outline the TFM technique used to compute cell traction stresses, as well as the quantification scheme used to measure changes in the cell morphology.

2.1 MECHANICAL TESTING OF POLYACRYLAMIDE HYDROGELS

Polyacrylamide gels of different stiffness can be fabricated by varying the ratio of acrylamide monomers with respect to bis-acrylamide cross-linker, as mentioned above. For this study, the ratios we used for this experiment were 1:14.25 or 1:50 (Bis:Am) to fabricate stiff and soft gels, respectively. Despite other labs reporting of the mechanical properties from varying PAAM gels, we created gel specimens to conduct our own mechanical testing. The following procedure will outline the fabrication of these specimens, as well as the dynamic mechanical testing used to measure the elastic modulus.

Using a 15 mL centrifuge tube, appropriate volumes of ultrapure MilliQ water, bis-acrylamide (Bis), and acrylamide (Am) were added at ratios of either 1:14.25 or 1:50 (Bis:Am). For softer gels (ratio 1:50), 8.95 mL of water was mixed with 0.3 mL of 2%w/v Bis and 0.75 mL of 40% w/v Am, to reach a complete volume of 10 ml. For stiffer gels (ratio 1:14.25), 6.95 mL of

water was mixed with 1.75 mL of Bis and 1.25 mL of Am. The pre-polymerization solution was then thoroughly vortexed for a few seconds. After mixing, the solution was allowed to de-gas for 30 minutes in a desiccator under vacuum to ensure that no gaseous oxygen was present in the mixture. Degassing is a very important step in the fabrication of PAAM gels because oxygen will consume the $2SO_4$ free-radical molecules needed for gel polymerization[12].After degassing, a fresh solution of 10% w/v ammonium persulfate (APS; Bio-Rad) was made by dissolving 10 mg of solid APS in 100 μL of MilliQ water. 50 μL of the 10% APS solution was then added to the pre-polymerization solution. (APS is used as the oxidizing agent in the polymerization reaction because it spontaneously decomposes and forms free-radicals[12].) Lastly, 5 μL of N,N,N′,N′-Tetramethylethylenediamine (TEMED; Sigma-Aldrich, St. Louis, MO) was added to the solution to initiate the polymerization reaction. (TEMED catalyzes polymerization by increasing the rate at which free-radicals are formed by APS, as described above.) Immediately after the addition of TEMED, the entire (10 ml) volume of pre-polymerization solution was poured gently into a 100 mm-diameter plastic Petri dish. The solution was then allowed to polymerize completely for 60 min under vacuum. After polymerization, the sheet of PAAM was removed from the dish and placed in 1X phosphate buffer solution (PBS) overnight at 4°C to allow the gel to hydrate.

We then used a TA Instruments RSA-G2 Dynamic Mechanical Analyzer (DMA) to perform unconfined compression tests of 10 mm-diameter gel specimens. To create these specimens, we punched 10 mm-diameter cylindrical plugs from the sheets of PAAM and used a set of calipers to measure the precise diameter and thickness of each plug. All mechanical tests were performed at room temperature in a bath containing PBS. The storage modulus of each specimen was measured using an isothermal strain sweep. The modulus at 2% strain was used for

the comparison of soft gel samples, whereas the modulus at 0.2% strain was used for the comparison of stiff gel samples. For all samples, these strains remained in the linear elastic regime (see Fig. 14A).

2.2 GLASS COVERSLIP SURFACE TREATMENT

PAAM gels were fabricated on 31 mm-diameter glass coverslips to serve as substrata for 2D cell culture. The glass coverslips were silanized to generate either hydrophobic or hydrophilic coverslip surfaces. In order to silanize the glass, we first incubated the coverslips in a 0.1 N sodium hydroxide (NaOH) solution for 1 hr at room temperature. Next, the coverslips were removed one-by-one, rinsed sequentially in 3 beakers of deionized water, and dried with nitrogen gas. The hydroxylated coverslips were then divided in half, with one half to be hydrophilic and the others to be hydrophobic. To make hydrophobic slides, a 2% solution of dichlorodimethylsilane (DCDMS; Sigma-Aldrich, St. Louis, MO) was prepared in toluene (Sigma-Aldrich, St. Louis, MO). The coverslips were then slowly placed into the solution one at a time to guarantee the entire slide was in contact with the solution. The slides were then incubated for 30 min and rinsed individually by dipping in a beaker of methanol. Afterwards, to preserve the coating, the slides were placed in a labeled petri dish, sealed, and stored in a desiccator under vacuum. To make hydrophilic slides, the remaining coverslips were submerged in a solution of 2% (3-Aminopropyl)trimethyloxysilane (APTMS, Sigma-Aldrich, St. Louis, MO) in acetone and allowed to incubate at room temperature for 30 min. Each was then removed from the solution, rinsed by dipping once in a beaker filled with fresh acetone, and allowed to air dry. Once dry, the coverslips were placed immediately in a solution of 0.5% glutaraldehyde in 1X PBS and allowed to incubate for 30 min. After incubation, the slides were placed in a breaker of 1X PBS, dipped

one-by-one in a sequence of 3 beakers of deionized water, and then dried with nitrogen gas. The hydrophilic slides were then placed in a labeled Petri dish and stored in a desiccator under vacuum for future use.

2.3 POLYACRYLAMIDE GEL FABRICATION

Soft and stiff PAAM solutions were prepared in 1 mL volumes following the same procedure described previously (see Appendix A). Following the addition of APS and TEMED to the pre-polymerization solution, a 40 μL droplet of the PAAM solution was placed atop one of the 31 mm-diameter hydrophilic (amino-silanized) glass coverslips. Afterward, a hydrophobic (chloro-silanized) coverslip was placed carefully on top, causing the solution to spread out between the two coverslips in a thin layer (Fig. 8, left). This entire assembly was then placed in a desiccator under vacuum for 30 min until polymerization was complete (Fig. 8, middle). The glass coverslip sandwiches were then submerged in 1X PBS and stored at 4°C (Fig. 8, right).

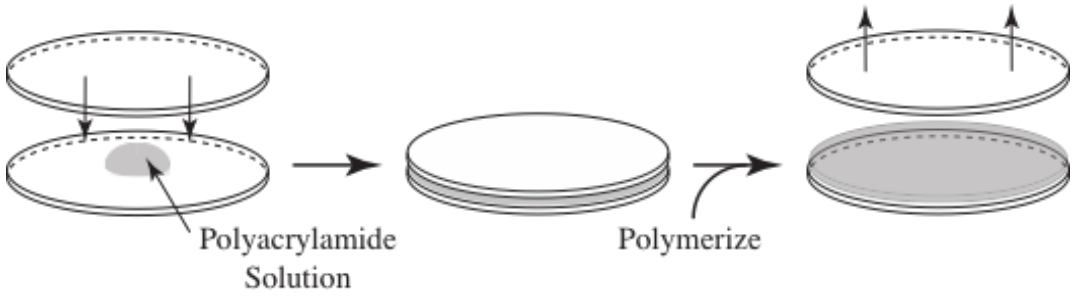

Figure 8. (left to right) Fabrication of polyacrylamide gel begins by placing a droplet of pre-gel solution on a hydrophilic, amino-silanized glass coverslip and sandwiching the droplet with a hydrophobic, chloro-silanized glass coverslip. The glass-gel-glass construct is then allowed to polymerize. Once polymerization is complete, the top slide can be easily removed leaving the exposed PAAM gel attached to the bottom coverslip.

2.4 POLYACRYLAMIDE FUNCTIONALIZATION

PAAM gels by themselves do not have binding sites for cell adhesion. Therefore, it was necessary that we functionalize the gel with using type I collagen to allow the corneal keratocytes

to attach and spread. Before functionalization, the hydrophobic top slides were removed using fine forceps, leaving the exposed hydrogel attached to the bottom slide. The gels were then brought into a biosafety hood, sterilized using 100% ethanol, and washed 3 times using sterile PBS. The PBS was then removed and replaced with a solution of 50 mM HEPES (Sigma-Aldrich, St. Louis, MO). Meanwhile, a 1 mg/mL solution of sulfo-SANPAH (Sigma-Aldrich, St. Louis, MO) was prepared in sterilized water. For each gel, 220 μL of the sulfo-SANPAH solution was pipetted onto the surface and spread evenly using a sterile pipette tip (Fig. 9, left). The gels were then exposed to ultraviolet light for ten minutes, washed once in HEPES and then placed in a new Petri dish. This process was repeated, gels were treated a second time with sulfo-SANPAH and washed 3 times with HEPES to remove any excess cross-linker. After sulfo-SANPAH treatment, the gels could be functionalized with type I collagen (Fig. 9, middle). The PAAM gels were thus placed in a 6-well plate and submerged in buffer until the collagen solution could be prepared.

For each 6-well plate, a total of 20 mL of collagen solution was prepared. Using a 50 mL centrifuge tube, 1.596 mL of 10X minimum essential media (MEM; Gibco, Gaithersburg, MD), 0.0416 mL of 0.1 M NaOH, and 18.02 mL of Dulbecco's modified eagle medium (DMEM; Sigma-Aldrich, St. Louis, MO) were mixed together. Lastly, 0.333 mL of a 3 mg/mL stock solution of PureCol type I bovine collagen (Advanced Biomatrix, San Diego, CA) was added to the mixture to reach a final collagen concentration of 50 μg/ml. The solution was then vortexed for 30 seconds at high speed. We removed the HEPES buffer from each well in the 6-well plate and replaced it with 3 mL of the 50 μg/ml collagen solution. The plate was placed into a humidified cell culture incubator at 37°C in an atmosphere containing 95% air and 5% CO_2 for 30 minutes. After incubation, the PAAM gels were washed twice with DMEM and then once with sterile HEPES.

The gels were then placed in DMEM and incubated at 37°C until it was time to plate the keratocytes (Fig. 9, right).

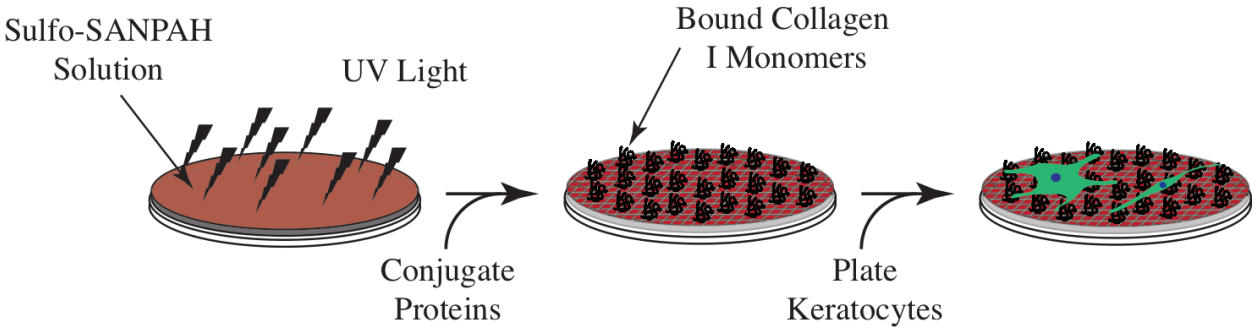

Figure 9. (left to right) Functionalization of polyacrylamide gels is done by covalently binding sulfo-SANPAH to the surface of the gel using UV light. Collagen I monomers are then covalently bound to the sulfo-SANPAH molecules on the surface of the gel. Keratocytes can then be plated on to the gels.

2.5 PRIMARY KERATOCYTE HARVEST AND CULTURE

6 days prior to culture, corneal keratocytes (NRK cells) were isolated from New Zealand White Rabbit eyes obtained from Pel-Freez (Rogers, AR, USA), as described previously[72] (Fig. 10). Upon arrival, the anterior portion of the cornea was wiped with an alcohol pad, and the corneal epithelium and Bowman's layer were removed using a sterile razor blade. Surgical scissors were then used to remove the cornea from the eye. Each cornea was carefully placed in fresh serum free media with the anterior side of the cornea facing downward to reveal the endothelium. Using a razor blade, the endothelial layer was then removed, leaving behind only the stroma and its residing keratocytes. The isolated corneas were then put into a 15 mL centrifuge tube containing digestion media overnight at 37°C inside a humidified incubator with 5% CO_2. The cells were then centrifuged and re-suspended in basal media containing DMEM supplemented with 1% RPMI vitamin mix (Sigma-Aldrich, St. Louis, MO), 100 µM nonessential amino acids (Invitrogen), 100 µg/ml ascorbic acid, and 1% penicillin/streptomycin. Only first passage cells were used for

experiments.

Prior to plating, serum free media, trypsin protease, and trypsin inhibitor were all warmed to 37°C in a hot water bath. NRKs were then brought into the tissue culture hood, the media from the flask was aspirated and washed with 2 ml trypsin. That trypsin was then quickly removed and replaced with another, fresh 2 mL of trypsin. The flask was then placed into the incubation chamber at 37°C for 2 minutes. After 2 min the trypsin had time to digest the proteins that adhere the cells to the flask, allowing for easy dissociation. After visualizing cell detachment, 8 mL of trypsin inhibitor was added to the tissue culture flask as soon as possible to prevent over-exposure of the cells to trypsin. The 10 mL of resulting solution in the flask was then pipetted and moved to a 15 mL tube and placed into a centrifuge where the cells were spun down for 4 min at a speed of 1500 rpm (385Xg). After centrifuging, the supernatant liquid of trypsin and trypsin inhibitor was aspirated out of the tube and replaced with 10 mL of warmed, serum free media. The pellet of NRKs was then re-suspended by gently pipetting up and down. Next, a 20 μL sample of cell solution was placed onto a hemocytometer to obtain the total cell count. The cells were once again spun down for 4 minutes in the centrifuge, the supernatant was aspirated and 2 mL of fresh serum free media was added to re-suspend the cells.

The NRK cells were plated on either collagen-functionalized PAAM gels or collagen-coated glass coverslips at 30,000 cells/ml. Each well in the 6-well plate received 2 ml media. After addition of cell culture media, the substrates were placed into an incubation chamber at 37°C with 5% CO_2. After 48 hours, new media was prepared for each experimental case, the old media was aspirated from the wells, and the new media was added to the wells. The 6-well plates were then replaced back into the incubator where they remained for the next 72 hrs. At day 5, the substrates

were removed from the incubator, the media was, aspirated and 1 mL of 3% paraformaldehyde (PFA) in PBS was added to fix the cells for immunofluorescence imaging.

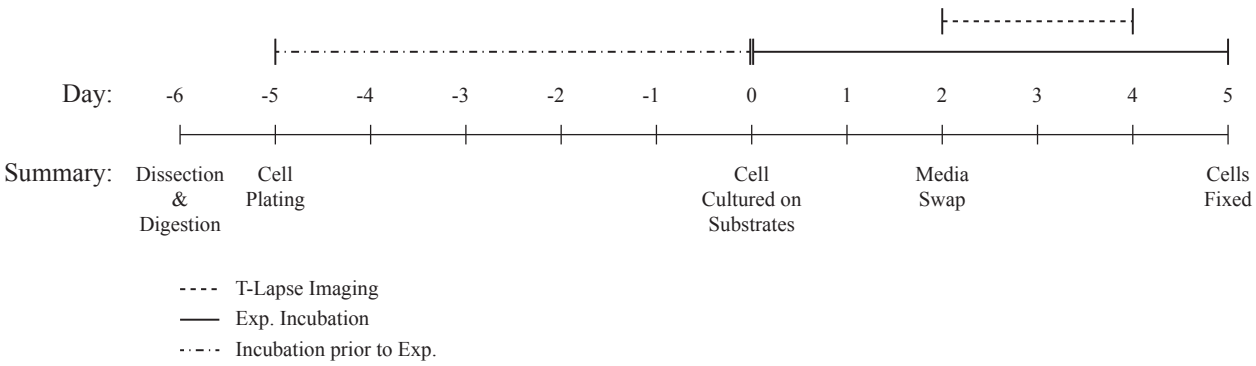

Figure 10. General timeline that describes the experimental process for NRK harvest and culture. NRK harvest occurs 6 days prior to cell culture (day -6). On day 0, cells are cultured on PAAM gels or glass coverslips. Following experimental culture, the cells are fixed after 5 days.

2.6 TIME-LAPSE MICROSCOPY AND IMMUNOFLUORESCENCE IMAGING

As mentioned above, in some experiments, the NRK cells were fixed after 5 days of culture using a 3% solution of PFA in PBS. The PFA crosslinks structures within the cells to enable their visualization via fluorescence microscopy. Cells were fixed for 20 minutes at room temperature and washed twice with PBS for 30 minutes on a shaker. All samples were then stored in PBS at 4°C for further processing.

Cells were then permeabilized for 30 min on a shaker using a 0.5 % solution of Triton X-100 in PBS. This surfactant creates pores in the cell membrane to enable the transport of antibodies and fluorescent labeling proteins into the cells. Following permeabilization, the NRK cells were treated with a blocking agent to minimize any non-specific binding of the labeling antibodies to other cellular components. For this step, a 1% bovine serum albumin fraction V (BSA, Equitech-

Bio Inc., Kerrville, TX) was prepared in 1X PBS. The samples were then incubated for 60 min on a shaker at room temperature in 1% BSA, and rinsed twice for 30 minutes in PBS.

For immunofluorescence imaging, the cells were then incubated at 37°C for 120 min with primary antibodies against either phosphorylated myosin light-chain (pMLC) (3675S; Cell Signaling, Danvers, MA) or α-smooth muscle actin (α-SMA) (A2547; Sigma-Aldrich, St. Louis, MO) at a 1:600 dilution, followed by a rinse in PBS for 60 min at room temperature on a shaker. Cells were then incubated with Alexa Fluor-conjugated secondary antibodies at a dilution of 1:200, along with Alexa Fluor 594 phalloidin (A12381; Invitrogen, Carlsbad, CA) at a dilution of 1:200 to label F-actin. Samples were then washed with 1XPBS for 60 min. Lastly, to stain for cell nuclei, cells were incubated at room temperature with DAPI (D9542; Sigma-Aldrich; St. Louis, MO) at a 1:1000 dilution for 20 min. Excess label was finally washed for 60 min with 1XPBS.

Confocal fluorescence images were then captured using a laser scanning confocal microscope (LSM 800; Zeiss, Jena, Germany) with either the 10×, 20×, or 40× (oil-immersed) objective. Images were then processed for image analysis using Zen software package.

We also conducted time-lapse microscopy experiments to compute the cellular traction exerted by cultured NRK cells over time. The experiments employed a technique known as traction force microscopy (TFM), described below, which uses the tracked motion of fluorescent beads embedded within the PAAM gel to estimate the cellular traction stresses. Owing to the relatively short working distance of our 20× objective, as well as the multi-well plate insert in our stage incubator, these time-lapse experiments required the construction of a modified 6-well plate (Fig. 11), which enabled up to 6 PAAM samples to be imaged in a single time-lapse experiment.

The customized 6-well plate was modified by first using a 31 mm diameter coverslip to trace a circle on the bottom of each well of the plate. Using the traced circles as a guide and a Dremel tool for boring holes, circles were then drilled and expanded into the plate several millimeters short of the previously sketched circle. The edges were then sanded down and polished using accessory drill bits from the Dremel toolkit. Next, because some wells required coverslips with PAAM gels for this experiment, either amino-silanized (and thereby hydrophilic) or untreated 31 mm glass coverslips were attached to the bottom of the 6-well plate over each hole. In order to "glue" the glass coverslips to the 6-well plate, polydimethylsiloxane (PDMS; Dow Corning, Midland, MI) at a ratio of 10:1 (elastomer silicon base:elastomer curing agent) was prepared to make a total weight of 5 grams. Using a transfer pipette, a thin outline of PDMS was carefully placed around the cut-out circle of each well. The treated and untreated glass coverslips were then gently placed over the holes and pressed down with forceps to ensure the coverslips were as level as possible. The dish was then placed in an 80°C oven upside down for 20 minutes to cure the PDMS. The dish was then taken out and tested for leaks by filling each well with MilliQ water and observing for several minutes. The dish was then emptied, dried, and placed into the desiccator for future use.

Gels were then fabricated and functionalized as previously described with one specific adjustment. For the TFM experiments, prior to gel fabrication, the 100 µL of deionized water was replaced with 100 µL of a concentrated suspension of fluorescent polystyrene microspheres (FluoSpheres, 0.2 µm; ThermoFisher, Waltham, MA). This suspension was created by diluting the stock solution of FluoSpheres with deionized water at a ratio of 1:4. The preparation of the PAAM pre-polymerization solution then proceeded as described above. We then placed 25 µL of the pre-

polymerization solution in each well with an amino-silanized (i.e., hydrophilic) glass coverslip. A smaller 18 mm chloro-silanized (i.e., hydrophobic) glass coverslip was place on top of the droplet. The PAAM was then allowed to polymerize for 30 min under vacuum.

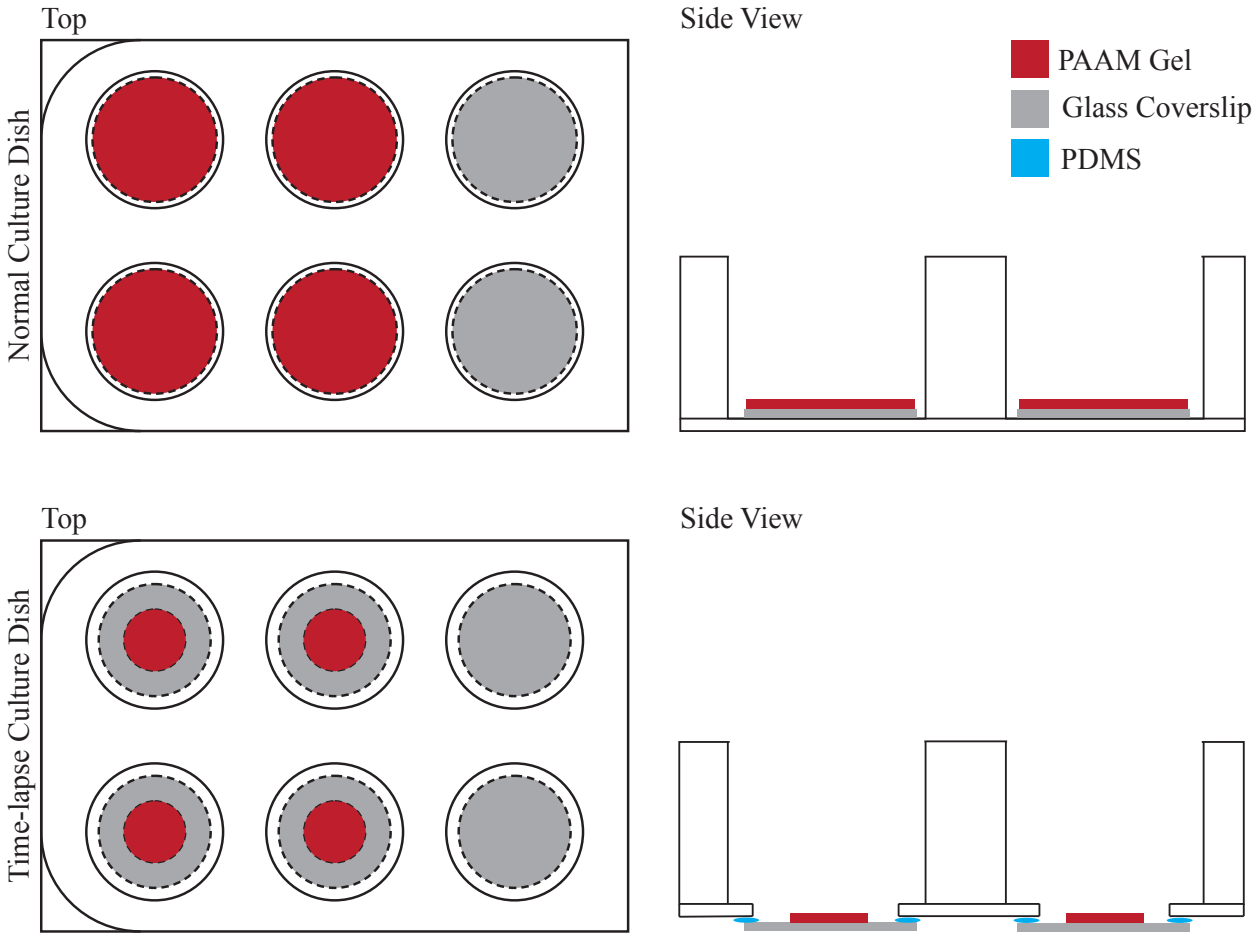

Figure 11. Comparison between the normal cell culture dish and our customized dish for fluorescent time-lapse and TFM experiments.

NRK cells were then plated on the PAAM substrates in the modified 6-well plates, as described above. After 48 hrs of culture, these plates were then transferred to a stage incubator (Incubator XL multi S1; Zeiss) on a Zeiss AxioObserver 7, equipped with a motorized stage, wide-field epifluorescence and phase contrast imaging capabilities, as well as the ApoTome.2 structured illumination module. During each time-lapse experiment, cells were incubated at 37°C in an

atmosphere containing 5% CO_2. For each substrate, 2 regions of interest (ROIs) were selected, and optically sectioned z-stacks of the fluorescent microspheres were captured, in addition to phase contrast images, every 30 minutes for 48 hours. At the end of the experiment, cells were lysed using a 5% solution of Triton X-100 in PBS to obtain a fluorescent z-stack of the undeformed configuration of the PAAM gel.

2.7 IMAGE QUANTIFICATION AND TRACTION FORCE MICROSCOPY

Confocal images of phalloidin staining were used to quantify differences in keratocyte morphology (Fig. 12, left column). Images were imported into Fiji (ImageJ). Next, cells that made junctions with one another were segmented and separated from one another. The red and blue channels were then split and converted to 8-bit images. Next, focusing on the red (phalloidin) channel, lower and upper bound threshold values were established such that the cell bodies were entirely filled and background noise was brought down to a minimum. This effectively makes a binary image of black cell bodies (Fig. 12, right column). Next, using the processing tool in ImageJ, the stack of images was "despeckled", thus making for a smoother cell outline and background noise was further reduced. With the cells separated, thresholds applied, and "despeckled", morphological characteristics could then be quantified. To assess cell spreading and cell elongation, the cell area, length, and aspect ratio were all analyzed using the "Analyze Particles" plugin in ImageJ. Morphological data was then summarized for each treatment condition and statistically evaluated for significance using Rstudio.

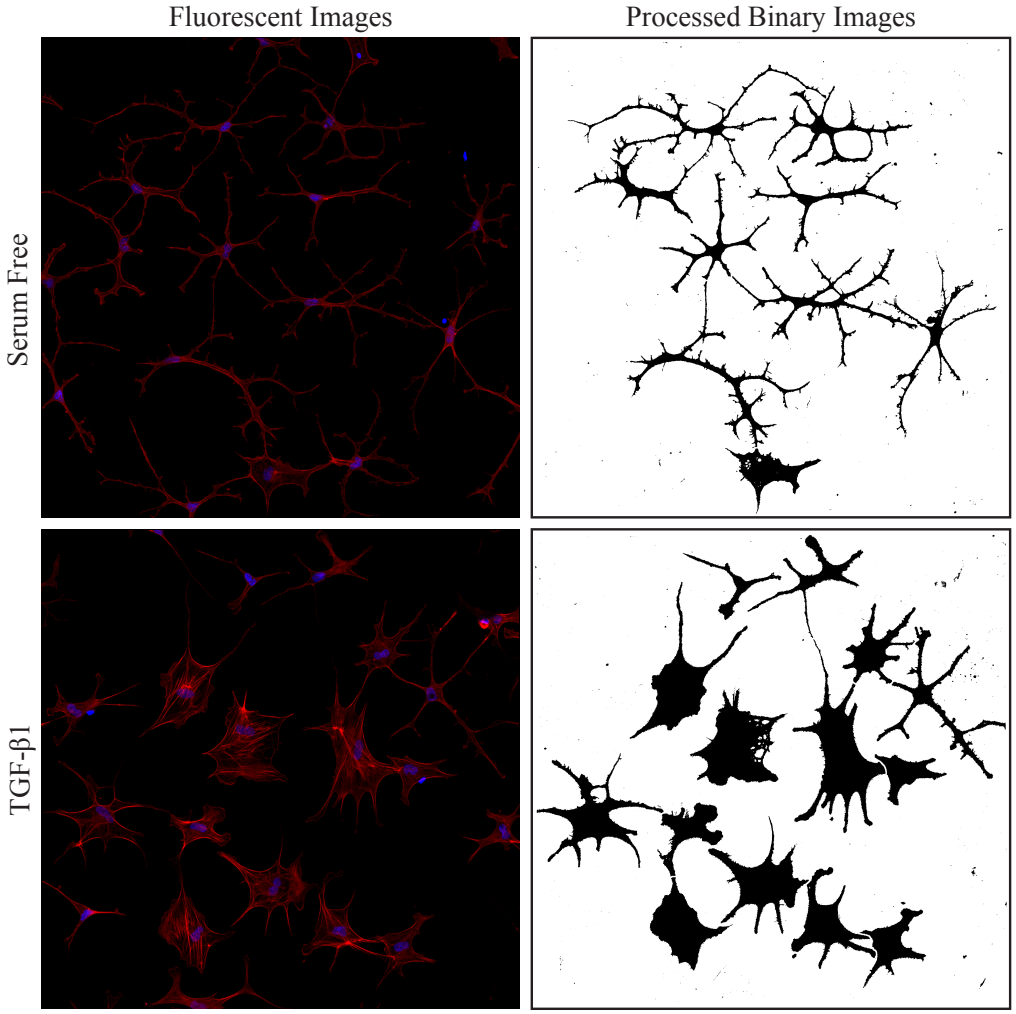

Figure 12. On the left, phalloidin (red) and DAPI (blue) staining for cells cultured on glass substrates in media with (bottom) and without (top) TGF-β1. On the right, is a processed, binary image outlining the cell body which will be used for quantification of the cellular morphologies.

When evaluating TFM experiments, each ROI from the time-lapse was evaluated for an individual cell's peak traction stress, net traction force, and temporal dynamic changes in contractility. To compute peak stresses and net forces, the most in-focus phase image of cells and beads closest to the surface of the gel were selected from the last frame of the time-lapse and undeformed z-stack. At each time point, the deformed bead image could be compared to the undeformed bead image to determine the deformation within the gel at that time (Fig. 13, top). The

two fluorescent bead images were aligned to one another using StackReg plugin in Fiji. Once aligned, all three images were merged together and characteristic cells were cropped from the ROI. Displacement maps were created using a Particle Image Velocimetry (PIV) plugin. In the PIV plugin, a window of a designated size compares the displaced and undisplaced bead images and, based on the bead movement, a vector with a calculated magnitude and direction is designated to the center of the windows location. The window will then examine the next area 15 pixels over and assign another vector based on the bead movement in that area. This is performed until the image has been fully analyzed (Fig. 13, bottom left). Next traction stress maps were then formed from the PIV using a Fourier Transform Traction Cytometry (FTTC) plugin in ImageJ[80] (Fig. 13, bottom right). Inputs of the FTTC included the pixel size (0.325 microns/pixel), poisson's ratio (assumed to be close to 0.5), Young's modulus which depended on whether the substrate was soft (1 kPa) or stiff (10 kPa), and regularization factor which was optimized the FTTC to lower background noise. Methods from Plotnikov et al were used to better our FTTC protocol and determine the ideal regularization factor[18]. To study dynamic changes in contractility, the same process was used at multiple time points from the time-lapse imaging. This analysis enabled us to generate dynamic traction force maps of keratocytes cultured on both soft and stiff PAAM gels under a variety of different experimental conditions.

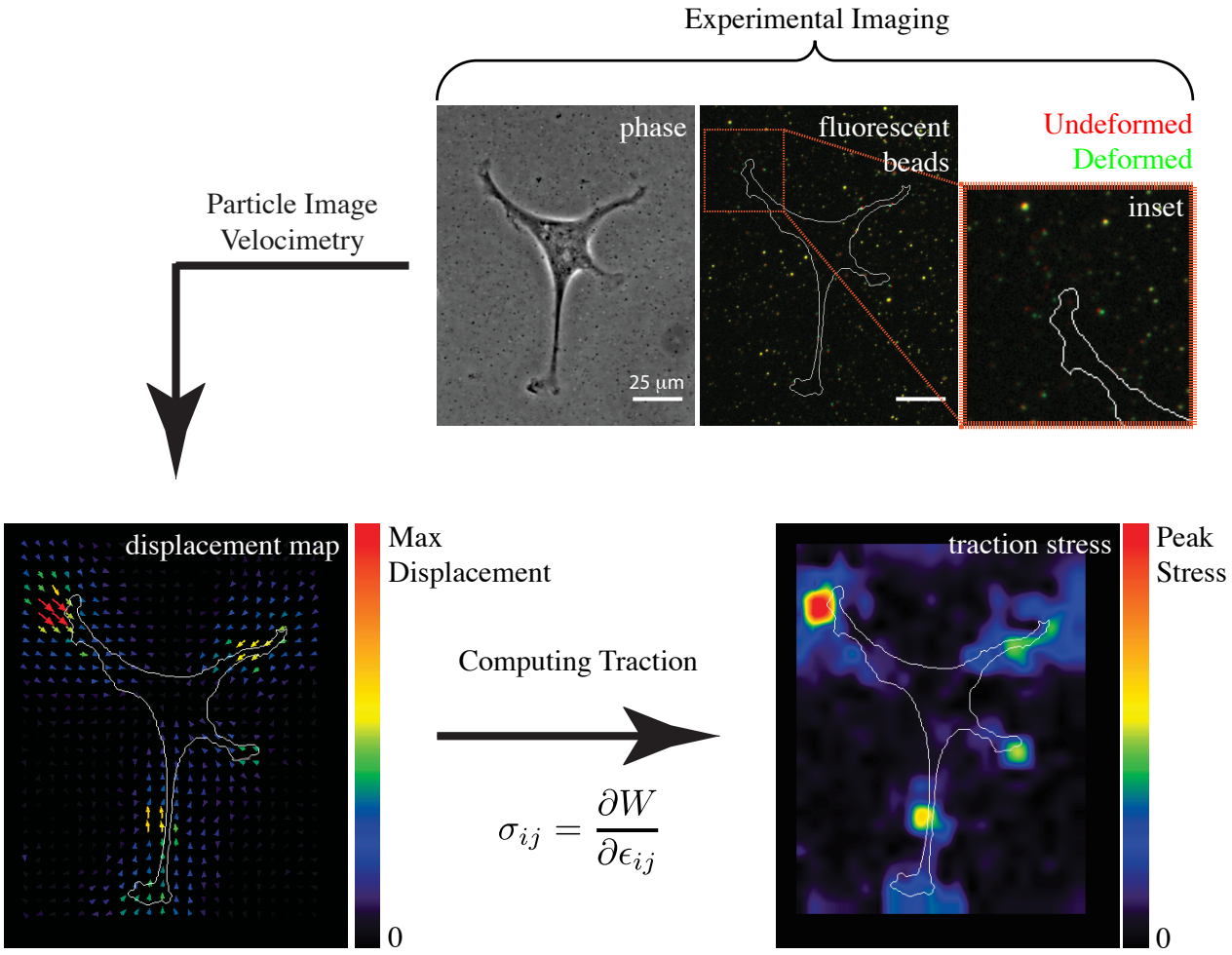

Figure 13. Schematic describing the process of quantifying traction stresses produced by a keratocyte. Using experimental bead images taken during and after time-lapse, displacement maps were produced by running a PIV analysis between the deformed and undeformed images. Using the displacement map, tractions could then be quantified by knowing the gel mechanical properties.

CHAPTER 3: RESULTS

3.1 TUNING POLYACRYLAMIDE GEL STIFFNESS

Our mechanical testing experiments revealed that the different preparations of PAAM produced gels with a storage modulus of either 11.21 ± 0.68 kPa or 1.16 ± 0.25 kPa (Fig. 14C), which were termed "stiff" and "soft," respectively. The loss modulus was significantly smaller than the storage modulus for both cases, indicating that gels behaved nearly elastically (Fig. 14A). The approximately constant storage modulus measured during the strain sweep suggested that the PAAM was in the linear elastic regime. As a result, we used 1 kPa and 10 kPa for the Young's modulus of the "soft" and "stiff" gels, respectively, as shown in Table 1. Comparing these values to normal and fibrotic stromal tissue, there is a clear similarity as normal and scar tissue having an elastic modulus of 1.1 ± 0.6 kPa and 10-20 kPa, respectively.

Table 1. Measured elastic moduli for PAAM gels with different relative concentrations of acrylamide and bis-acrylamide. Volumes of acrylamide, bis-acrylamide, deionized water, APS and TEMED should all add up to approximately 1 ml.

Elastic Modulus	H_2O	40% Acrylamide	2% Bis-Acrylamide	TEMED	APS
1,000 Pa	695 µL	75 µL	30 µL	0.5 µL	5 µL
10,000 Pa	895 µL	125 µL	175 µL	0.5 µL	5 µL

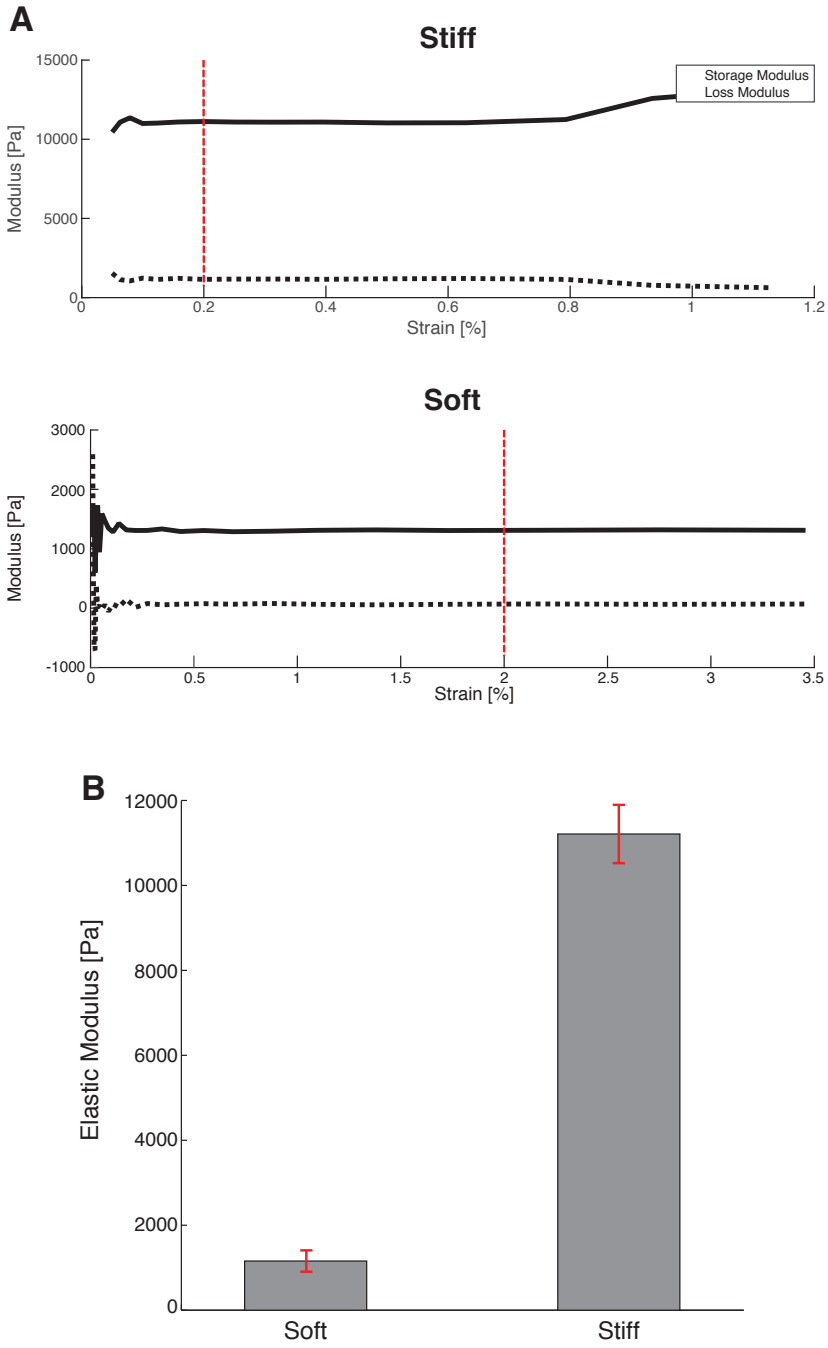

Figure 14. (A) DMA results for a characteristic soft (bottom) and stiff (top) PAAM gel. The storage modulus (black solid line) and loss modulus (black dashed lines) were analyzed as a function of strain. The plateaued state of each plot signifies the linear elastic regime. From this area we obtain our elastic modulus (dashed red line). (B) Average elastic modulus for soft and stiff gel were measured from n=9 specimens for 3 different experimental replicates for both soft and stiff PAAM gels.

3.2 SUBSTRATE STIFFNESS INFLUENCES KERATOCYTE MORPHOLOGY

NRK cells were cultured on either 1 kPa or 10 kPa PAAM gels, or glass coverslips, that were functionalized with type I collagen. In serum free conditions, NRKs cultured on glass coverslips exhibited a morphology characteristic of a quiescent keratocyte phenotype after 5 days of culture. The cells exhibited thin dendritic processes extending outward from the cell body. As the stiffness of the substratum decreased, however, the number and length of these processes decreased (Fig. 15A-C). In the presence of TGF-β1, the cells on both glass coverslips and 10 kPa PAAM gels exhibited phenotypes indicative of myofibroblastic transformation. The cells were spread out with broad morphologies and clearly visible stress fibers (Fig. 15E,F). On 1 kPa substrata, however, the TGF-β1-treated cells exhibited strikingly different morphologies. In this case, the cultured NRKs displayed less cell spreading, formed long, thin cellular extensions, and exhibited few stress fibers, behaviors indicative of a more quiescent keratocyte (Fig. 15D).

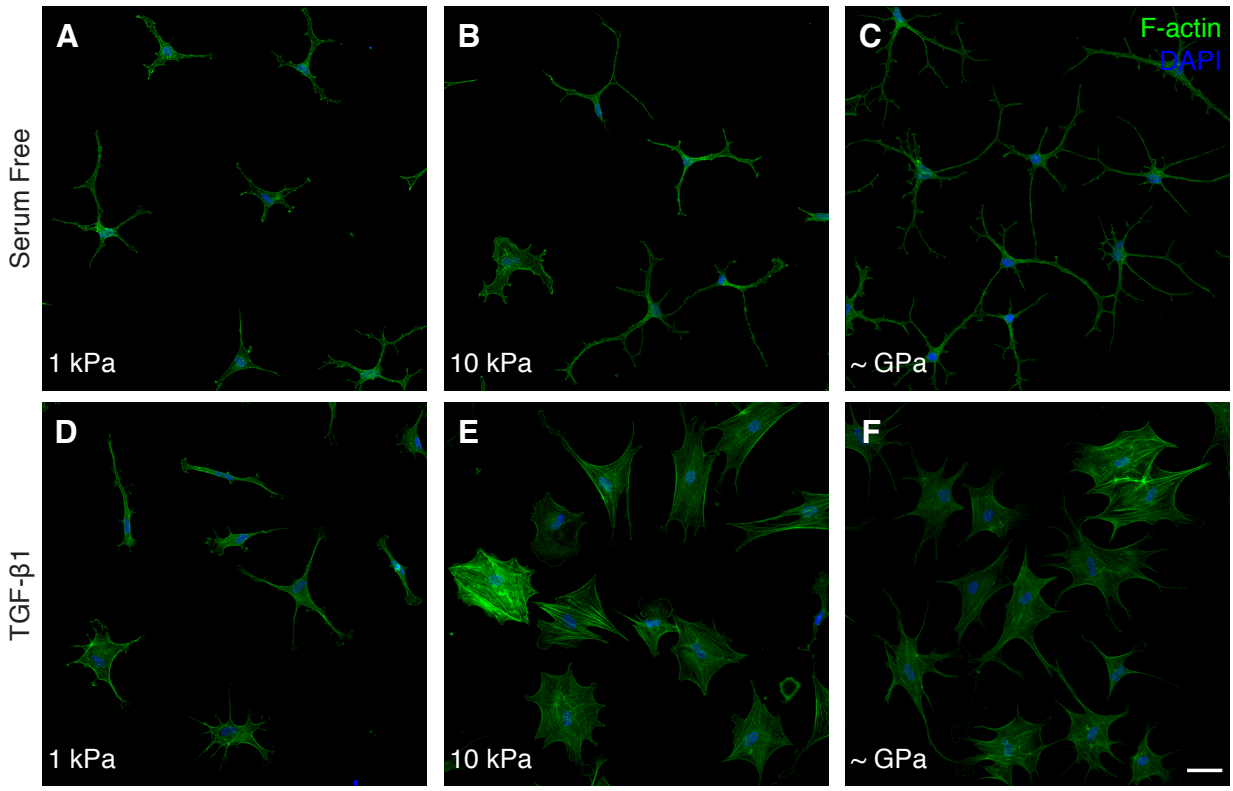

Figure 15. Characteristic confocal fluorescence images of fixed corneal keratocytes cultured on either 1 kPa (A and D) or 10 kPa (B and E) polyacrylamide gels, or glass (C and F) coverslips, functionalized with. Prior to fixation, cells were cultured in either serum free media (A-C) or media containing TGF-β1 (D-F) for 5 days. Keratocytes were stained using phalloidin (green) and DAPI (blue) to visualize F-actin and nuclei, respectively. Scale bar is 50 μm.

Quantitative measurements of cell morphology showed significant differences in cell area, cell length, and cell aspect ratio. In the presence of TGF-β1, NRKs on soft (1 kPa) substrates showed a significant decrease in cell area and length, when compared to cells cultured on glass coverslips. On stiff PAAM gels, NRKs spread less than cells plated on glass coverslips; however, they were significantly more spread than cells on soft PAAM gels. A significant increase in aspect ratio was seen when cells were plated on soft gels, which suggested an increase in cell elongation. When the cells were cultured in serum free media, morphological phenotypes were relatively similar regardless of substrate stiffness. The largest differences were seen in cell length, where on soft and stiff PAAM gels the cells were significantly smaller than those on glass coverslips (Fig. 16).

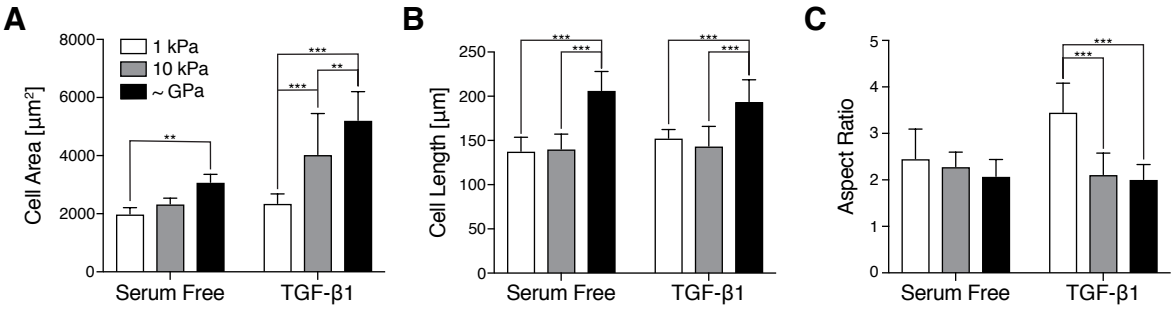

Figure 16. Quantification of projected cell area (A), cell length (B), and cell aspect ratio (C). Mean ± s.d. is shown for n=9 substrates from 5 experimental replicates. A two-way ANOVA with a Tukey post-hoc test was used to evaluate significance between groups. (*, $p < 0.05$; **, $p < 0.01$; ***, $p < 0.001$).

3.3 SUBSTRATE STIFFNESS MODULATES KERATOCYTE ACTIVATION

To determine if differences in substratum stiffness were modulating levels of myofibroblastic activation, we stained cultured NRKs for α-SMA immunofluorescence, a marker protein for myofibroblasts[81]. The number of α-SMA-positive cells were then quantified for each experimental condition. In serum free media, negligible amounts of α-SMA were observed, regardless of the stiffness of the underlying substratum, indicating extremely low levels of activation, as expected (Fig. 18, left bars). When cells were cultured in the presence of TGF-β1, on either stiff PAAM gels or glass coverslips, the percentage of α-SMA-positive cells increased significantly (Fig. 17), indicating elevated levels of myofibroblastic transformation. On soft PAAM gels, however, even when treated with TGF-β1, the fraction of α-SMA positive cells decreased significantly, suggesting that sufficiently compliant microenvironments are capable of suppressing the myofibroblastic activation of corneal keratocytes (Fig. 18). It is also worth noting there was not a significant difference between NRKs cultured in media with TGF-β1 on soft PAAM gels compared to any of the substrates cultured in serum free media. This suggests quite a significant knock down in the activation to a myofibroblasts.

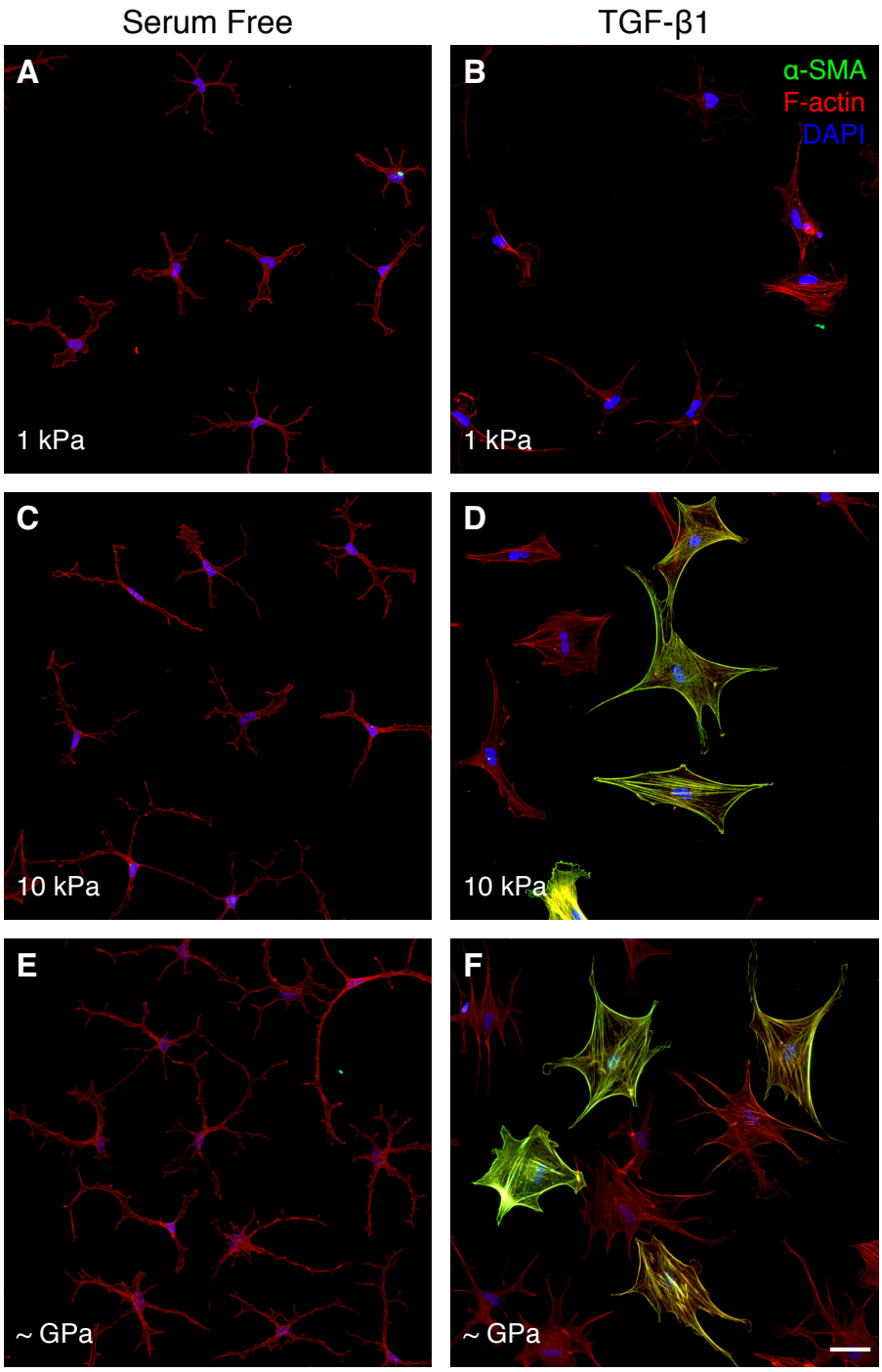

Figure 17. (A-F) Characteristic confocal immunofluorescence images of fixed corneal keratocytes cultured on either 1 kPa (A and B) or 10 kPa (C and D) polyacrylamide gels, or glass (E and F) coverslips. After fixation, keratocytes were stained using phalloidin (red), DAPI (blue), and anti-α-SMA antibody (green) to visualize F-actin, cell nuclei and α-SMA, respectively. Scale bar is 50 μm.

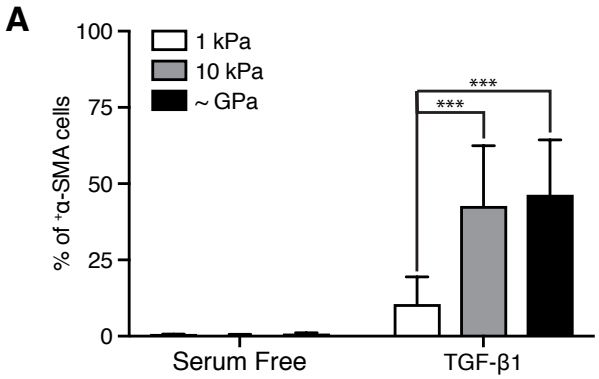

Figure 18. (G) Quantification of the percentage of keratocytes that were positive for the myofibroblastic marker, α-SMA. Mean ± s.d. is shown for n=16 substrates from 4 experimental replicates. A two-way ANOVA with a Tukey post-hoc test was used to evaluate significance between groups. (***, $p < 0.001$).

3.4 SUBSTRATUM STIFFNESS CONTROLS CONTRACTILE PHENOTYPE OF CULTURED KERATOCYTES

To better understand how ECM stiffness influences the contractile behavior of NRKs in the presence (or absence) of TGF-β1, we stained cells that were fixed after 5 days of culture for phosophorylated-myosin light chain (pMLC) immunofluorescence, which allows us to visualize regions of active contractility within the cells. On stiff PAAM gels or glass coverslips, NRKs cultured in the presence of TGF-β1 exhibited broad pMLC immunofluorescence across the cell body, with pMLC localized primarily along stress fibers that traversed the cell body (Fig. 19 C-F). Interestingly, cells cultured on soft PAAM gels, showed a strikingly different subcellular localization pattern, even when treated with TGF-β1. pMLC immunofluorescence was concentrated primarily at the distal tips of extended cellular processes with only low levels present in the main cell body (Fig. 19A,B). These results suggest that the stiffness of the physical microenvironment is sufficient to modulate the subcellular distribution of contractility within the cultured cells. In serum free conditions, cells exhibited very low levels of pMLC immunofluorescence on all substrata. When detected, however, pMLC was localized mainly at the

tips of cellular processes (see Appendix B, Fig. B4), similar to the behavior of cells cultured on soft PAAM gels in the presence of TGF-β1. Taken together, these data suggest that NRKs treated with TGF-β1 retain a quiescent phenotype than those cultured on stiffer substrata.

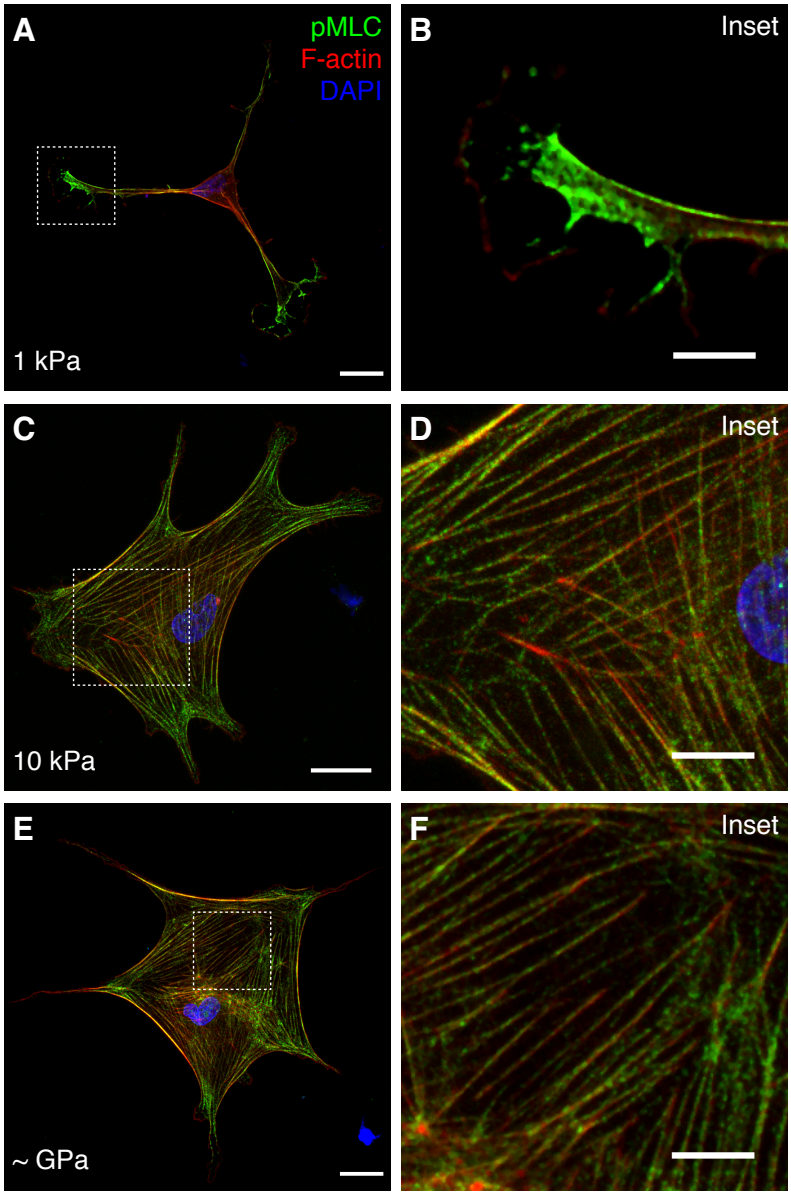

Figure 19. (A-F) Confocal immunofluorescent images of fixed corneal keratocytes cultured on either soft (A) or stiff (B) polyacrylamide gels, or glass (C) coverslips. Scale bars, 25 μm. After fixation, keratocytes were stained with phalloidin (red), DAPI (blue), and anti-pMLC antibody (green) to visualize F-actin, cell nuclei, and phosphorylated myosin light chains, respectively. For the inset images, the scale bars are 10 μm.

Although pMLC immunofluorescence provides information regarding subcellular regions of contractility, it is not a proxy for the magnitude or distribution of traction forces exerted by the cell. We therefore performed traction force microscopy experiments to determine how patterns of contractile traction forces were modulated by changes in substratum stiffness. Using Fluorescent time-lapse microscopy, we were able to capture dynamic deformations of the PAAM gel by tracking the displacement of embedded fluorescent microspheres as NRKs pulled on the substrate. From these deformations to an undeformed bead image taken after the time-lapse, we were able to quantify the peak traction stresses and net traction forces being implemented by a cell using image processing plugins in FIJI, as described previously. Since bead displacements are needed to quantify cell contractility in TFM experiments, neither stress nor strain were quantified for cells on glass coverslips.

After 4 days of culture, we observed striking differences in the contractile behavior of the cells treated with TGF-β1 but not amongst cells cultured in serum free conditions. In serum free conditions, the cells on soft or stiff substrates exerted very low, near-zero stresses (Fig. 20A,B & Fig. 21). When NRKs were treated with TGF-β1, however, cells cultured on stiff PAAM gels exhibited a significant increase in both the peak traction stress, as well as the net contractile force. Interestingly, when cells were cultured on soft PAAM gels in the presence of TGF-β1, this striking increase in peak traction stress and net contractile force were not observed. The peak contractile stress exerted by the NRKs on soft PAAM gels approached the values observed in cells under serum free conditions. In addition, there was a relatively large variance in the peak contractile stress exerted by TGF-β1-treated keratocytes cultured on stiff PAAM gels, owing to the fact that some cells exhibited peak contractile stresses nearly an order of magnitude above the average. The

total net contractile force exerted by the cells, which was obtained by integrating the magnitudes of the traction stress across the cell body, showed similar trends.

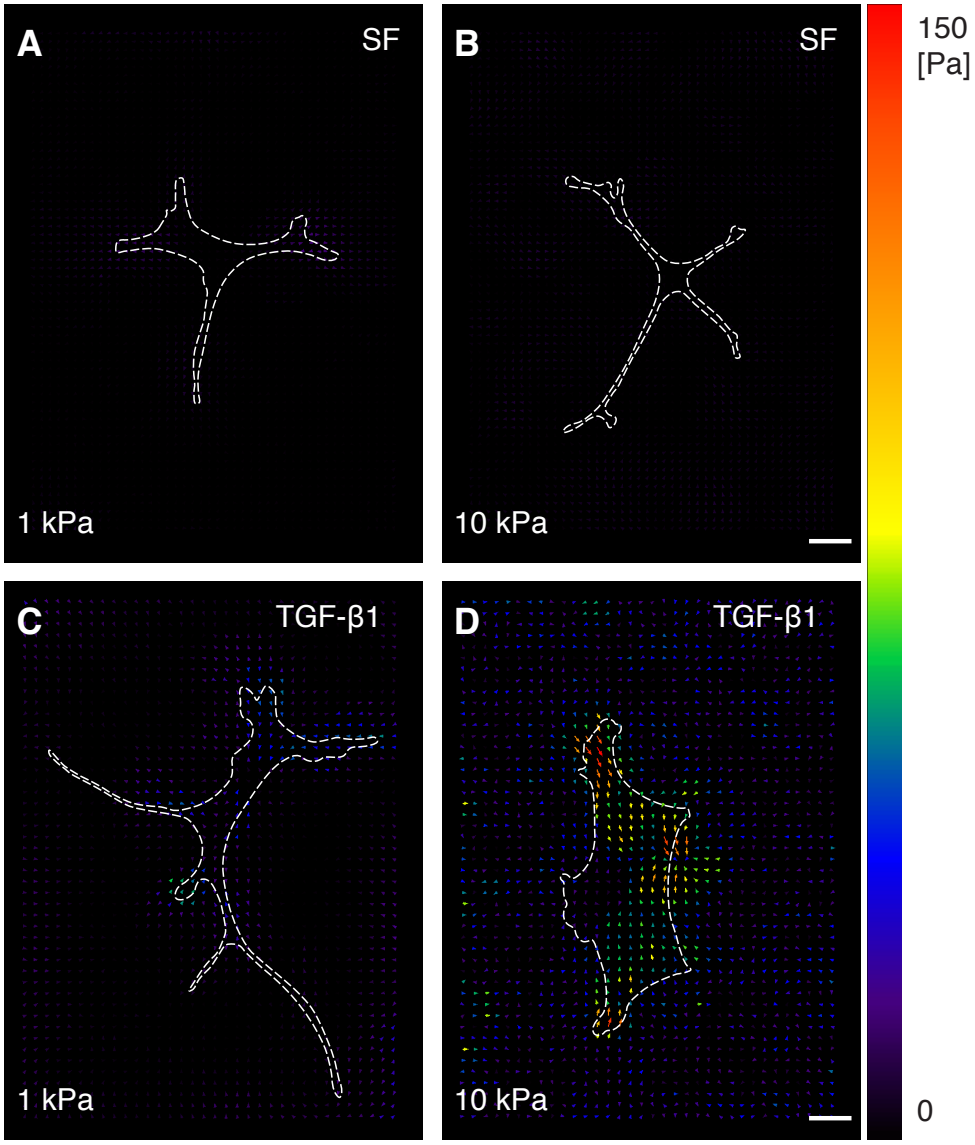

Figure 20. (A-D) Representative traction stress maps for cells on 1 kPa (A and C) and 10 kPa (B and D) polyacrylamide gels with (C and D) and without (A and B) TGF-β1. Cell outlines are marked by the white dashed line. Scale bars are 25 μm.

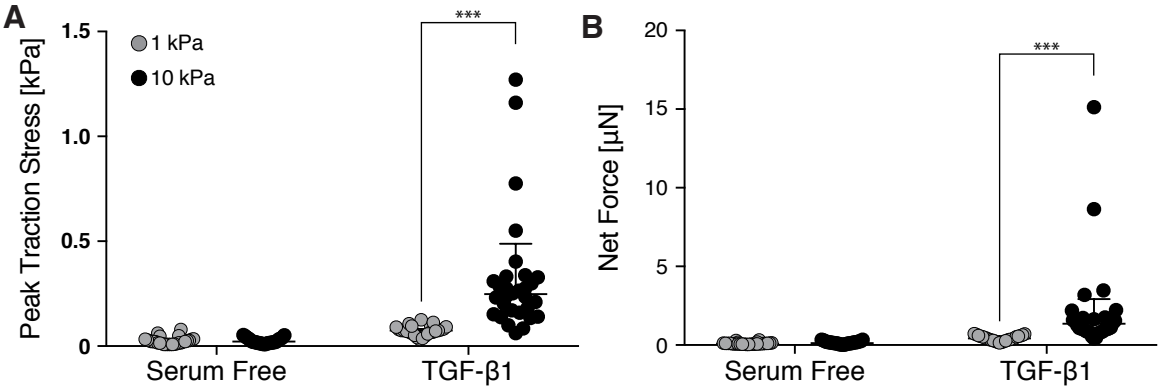

Figure 21. Cloud plots showing peak traction (A) stresses and net traction force (B) for individual cells on either soft (grey dots) or stiff (black dots) in media with and without TGF-β1. Mean ± s.d. is shown for n=5 substrates from 5 experimental replicates. A two-way ANOVA with a Tukey post-hoc test was used after applying a logarithmic transformation to the dataset to evaluate significance between groups. (***, $p < 0.001$).

There were also striking differences in the spatial distribution of contractile traction stresses between the experimental conditions. After 4 days of culture, cells cultured on soft PAAM gels and treated with TGF-β1 had traction stresses localized mainly at the tips of elongated cellular extensions, whereas on stiff PAAM gels the traction stresses were often distributed across a larger fraction of the cell body. In serum free conditions, cells would also exert stresses at the distal tips of processes, similar to that of cells on soft substrates in the presence of TGF-β1. These distributions are in accord with the patterns of pMLC immunofluorescence observed in Fig. 19. Even so, on stiff PAAM gels, areas of the highest traction stress were present typically along the boundary of cells treated with TGF-β1. These regions may perhaps be associated with mature focal adhesions.

These data provide only a snapshot of the contractile behavior of keratocytes after 4 days of culture, so we also performed dynamic traction force microscopy experiments between 2 and 4 days of culture to determine how the patterns of contractile tractions stresses evolve over time

(Fig. 22). (This time-frame was selected to capture the transition of the cultured NRKs to a myofibroblastic phenotype in presence of TGF-β1.) When treated with TGF-β1, cells on soft PAAM gels displayed relatively low contractile stresses (~30-40 Pa) at 48 hours, in a pattern redolent of that observed in Fig. 20C. During the time-lapse experiment, the cells began to extend and retract its elongated cellular processes in a strikingly dynamic fashion but continued to exert traction stresses in the same regime as at earlier time-points. Even after 4 days (96 hours) of culture, there was no significant increase in magnitude of the exerted contractile stresses (Fig. 22D-F).

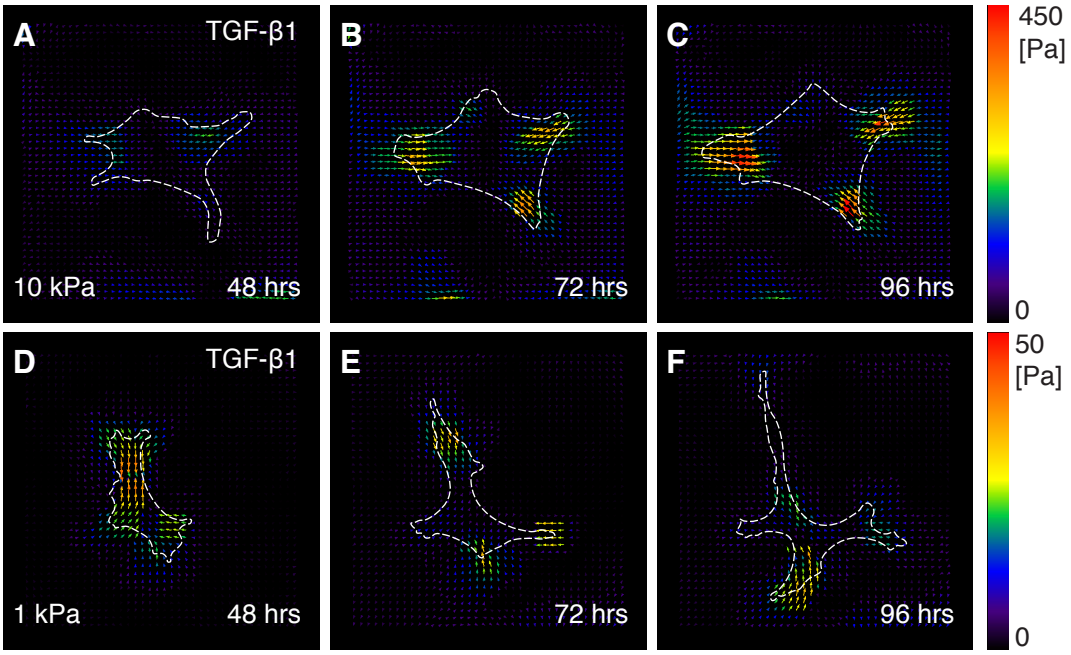

Figure 22. (A-F) Representative traction stress maps of a single corneal keratocyte at 48 (A & D), 72 (B & E) and 96 (C & F) hours on either 1 kPa (D-F) or 10 kPa (A-C) polyacrylamide gels in the presence of TGF-β1. Cell outlines are marked by the white dashed line.

Cells cultured in the presence of TGF-β1 on stiff PAAM gels, on the other hand, showed a striking increase in the magnitude of their contractile traction stresses over time. Initially, at 48 hours, the cells pulled against the substratum with stresses on par with their counterparts on soft

PAAM gels. By 72 hours, however, the contractile stresses began to increase significantly, and by 96 hours the stresses have increased in some cases to values greater than 400 Pa. Moreover, overtime on stiff substrates, the patterns of contractility remain relatively the same for the full 48 hours time-lapse, however, on soft substrates there appears to be significantly more variability in contractile patterns.

3.5 INHIBITION OF KERATOCYTE CONTRACTILITY

To determine how contractility might affect the stiffness-dependent myofibroblastic activation of cultured NRK cells, we treated keratocytes with TGF-β1 as well as the non-muscle myosin II inhibitor blebbistatin. After 5 days of culture, phalloidin-stained images of fixed cells revealed several distinct differences in cell morphology. As a control, NRKs treated with TGF-β1 alone displayed characteristics typical of myofibroblasts when cultured on stiff PAAM gels or glass coverslips: broad cellular processes, the formation of stress fibers, and increased cell area. Meanwhile, consistent with our results above in Fig. 15 on soft PAAM gels, the cultured NRK cells exhibited features more indicative of a quiescent phenotype: decreased cell area, the absence of stress fibers, thin elongated processes extending outward from the cell body. When treated with blebbistatin, however, these stiffness-dependent differences in morphology and stress fiber formation decreased significantly (Fig. 23D-F). On all substrata, the cells no longer formed stress fibers and displayed dendritic morphologies more characteristic of quiescent keratocytes. In a few instances, individual cells possessed broad cellular processes, but spread out less than controls and formed significantly fewer stress fibers.

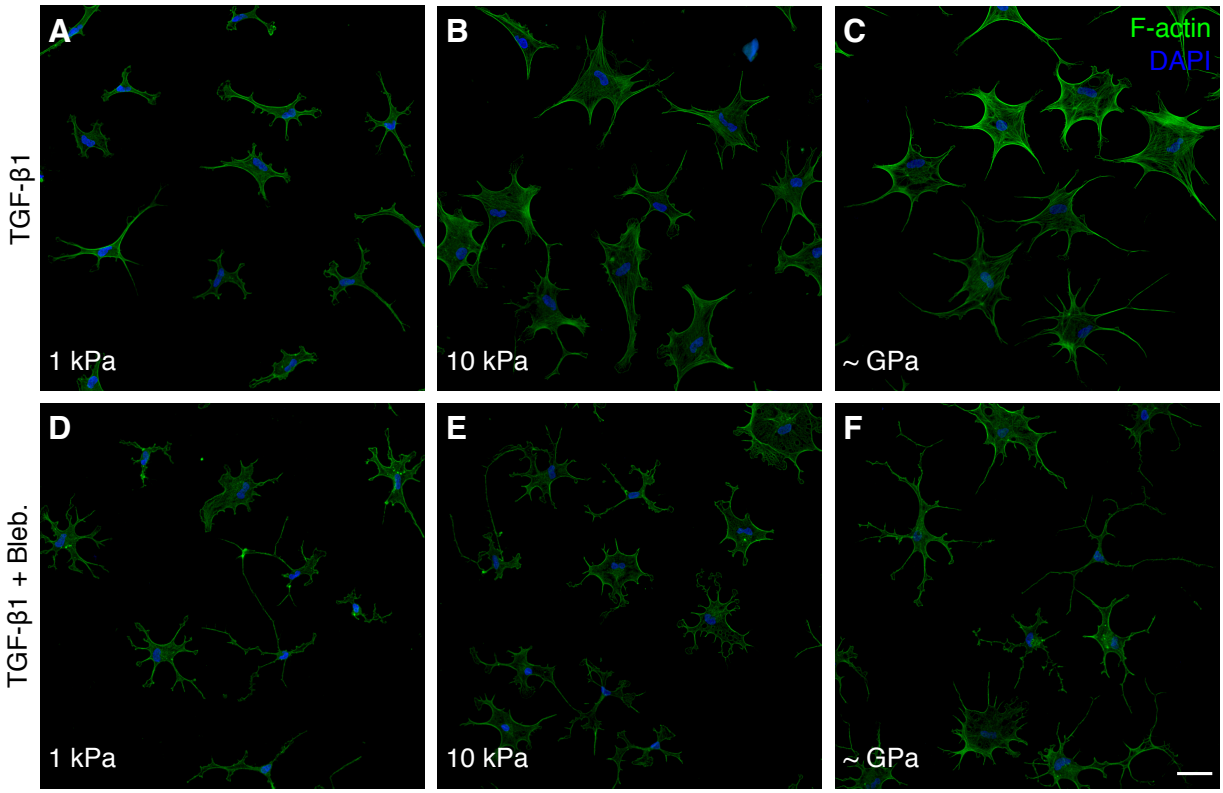

Figure 23. Characteristic confocal fluorescence images of fixed corneal keratocytes cultured on either 1 kPa (A and D) or 10 kPa (B and E) polyacrylamide gels, or glass (C and F) coverslips, functionalized with 50 μg/mL type I collagen monomers. Prior to fixation, cells were cultured in either media containing TGF-β1 with (D-F) or without (A-C) 20 μM blebbistatin for 5 days. Keratocytes were stained using phalloidin (green) and DAPI (blue) to visualize F-actin and nuclei, respectively. in the presence of TGF-β1, keratocytes morphologies are similar to that observed in Figure 1 (D-F). However, when blebbistatin is added to the media along with TGF-β1, cells morphologies were more dendritic in shape and stress fibers were absent. Scale bar is 50 μm.

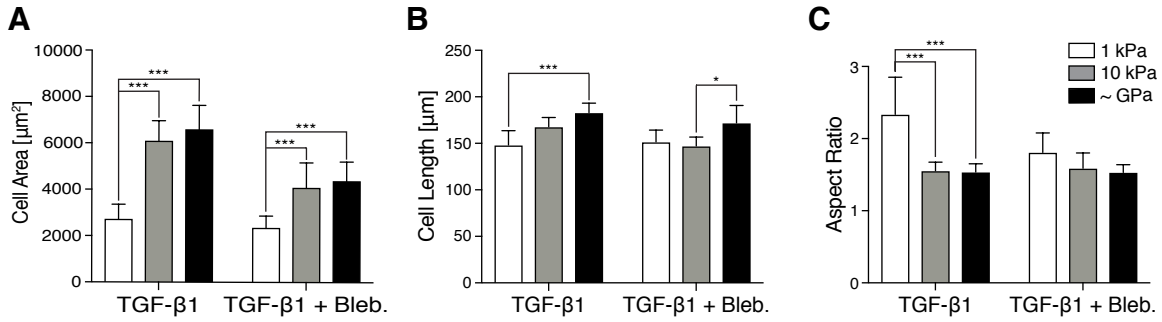

Figure 24. (A-C) Quantification of projected cell area (A), cell length (B), and cell aspect ratio (C) revealed that in the presence of TGF-β1 with blebbistatin, morphology differences were significantly lower than those in media without blebbistatin. Mean ± s.d. is shown for n=8 substrates from 3 experimental replicates. A two-way ANOVA with a Tukey post-hoc test was used to evaluate differences between groups. (*, $p < 0.05$; **, $p < 0.01$; ***, $p < 0.001$).

Cellular morphologies were quantified as in Fig. 24. In all cases, treatment with blebbistatin produced smaller differences in cell area, length, and aspect ratio amongst NRKs cultured on substrata of different stiffness (Fig. 24). In addition, on stiff PAAM gels and glass coverslips, the measured cell area decreased significantly when treated with blebbistatin. Interestingly, however, on soft PAAM gels, the cell areas were unchanged by the inhibition of contractility. Treatment with blebbistatin also abolished any stiffness-dependent differences in cell elongation, a result similar to that observed in cells cultured in serum free conditions (Fig. 16).

We also performed TFM experiments to determine how treatment with blebbistatin influenced the distribution of cellular traction forces. As expected, traction stress maps for characteristic cells showed decreased stresses for NRKs treated with blebbistatin (Fig. 25, bottom row). As observed above (Fig. 20), NRKs were treated with TGF-β1 alone produced stresses on stiff PAAM gels that were significantly higher than those produced by cells on soft substrata. These stiffness-dependent differences in contractile traction stresses, however, were abrogated completely in cells treated with blebbistatin (Fig. 25). Interestingly, when treated with blebbistatin

stresses are localized at tips of cellular extensions, similar to results from cells in serum free conditions, as described above.

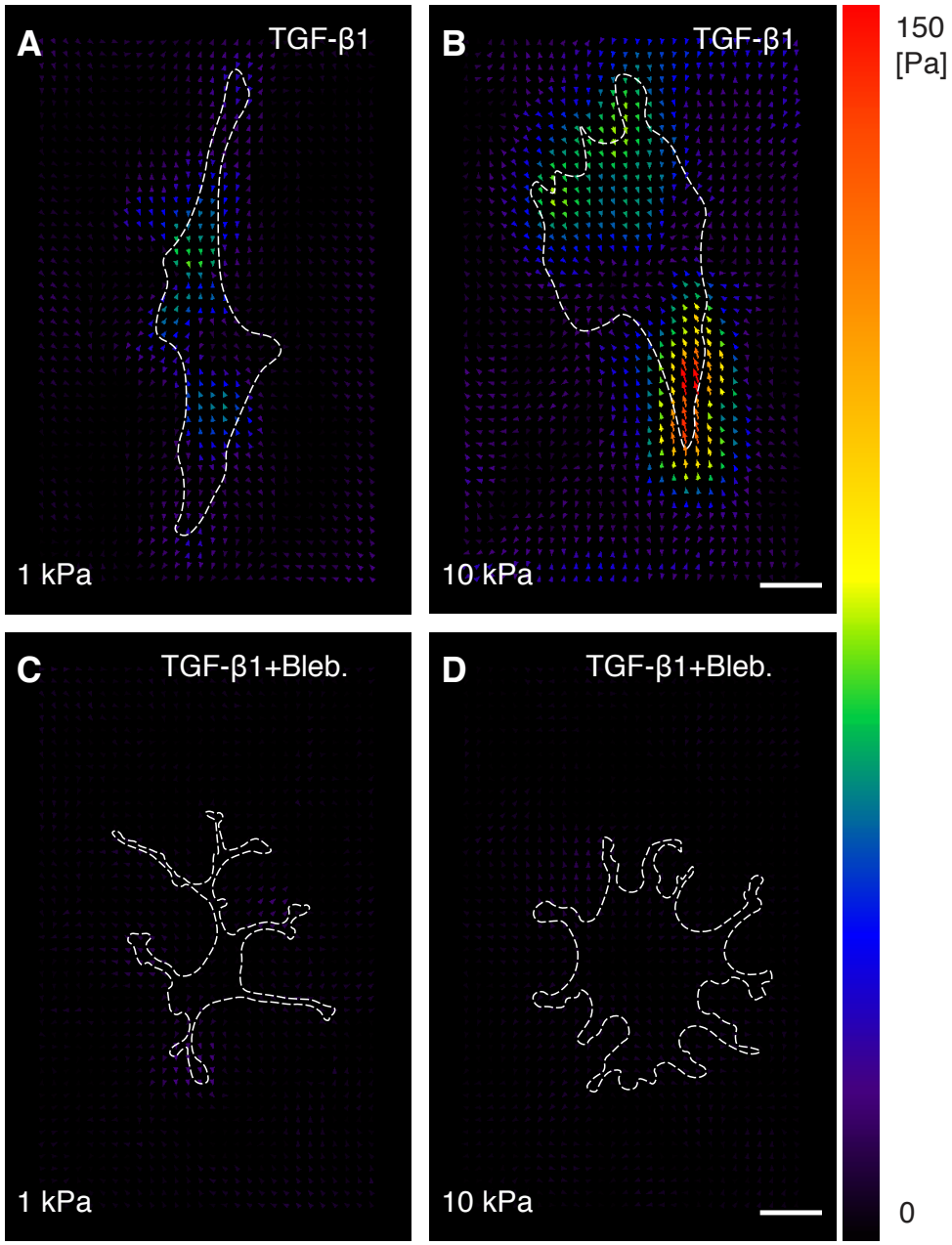

Figure 25. (A-D) Representative traction stress maps for cells on 1 kPa (A and C) and 10 kPa (B and D) polyacrylamide gels cultured with TGF-β1 with (C and D) and without (A and B) 20 μM blebbistatin. Cell outlines are marked by the white dashed line. Scale bar is 25 μm.

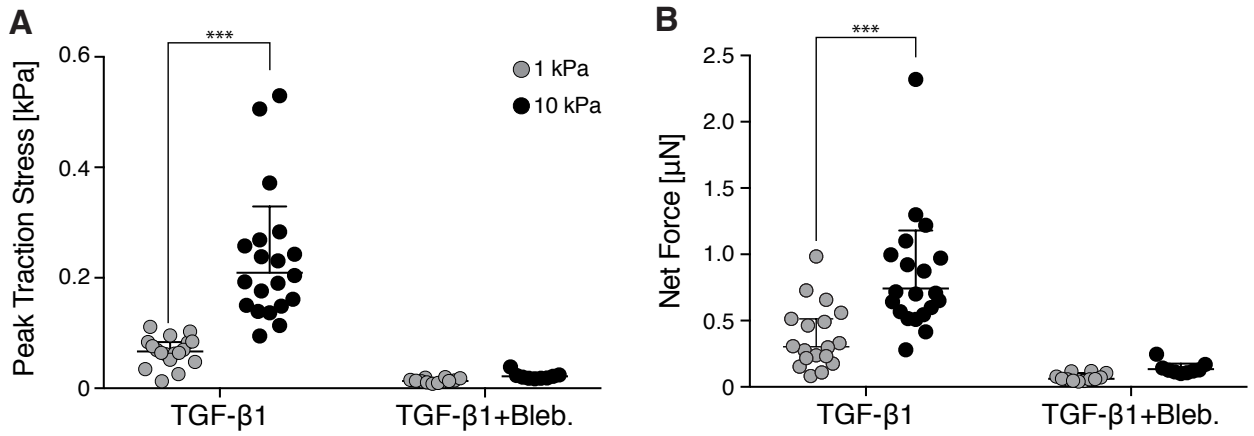

Figure 26. Cloud plots showing peak traction (A) stresses and net traction force (B) for individual cells on either soft (grey dots) or stiff (black dots) in media with TGF-β1 supplemented with and without 20 μM blebbistatin. Geometric mean ± s.d. is shown for n=5 substrates from 3 experimental replicates. A two-way ANOVA with a Tukey post-hoc test was used to evaluate significance between groups. (***, $p < 0.001$).

Quantification of peak traction stress and net cellular contractile force corroborated these qualitative observations (Fig. 26). Inhibiting contractility with blebbistatin produced a significant drop in the peak traction stress, independently of whether the cells were cultured on stiff or soft PAAM gels. It is interesting to note that the peak traction stress exerted by NRKs treated with blebbistatin and TGF-β1 simultaneously was similar to that exerted by cells cultured in serum free conditions (Fig. 21). Similar trends were observed by comparing the net contractile force generated by the cultured cells (Fig. 26B). Taken together, these results suggest that inhibiting contractility is sufficient to disrupt the stiffness-dependent myofibroblastic activation of cultured NRKs.

Taken together, the results show that when plated on stiff gels or glass coverslips in the presence of TGF-β1, cells will display broad morphologies, with abundant stress fibers, and pMLC localization occuring along the stress fibers within the cell. However, on soft gels, the cells become more elongated and less spread, forming few stress fibers, and pMLC is localized at the distal tips of cell extensions. Also on stiffer substrates in TGF-β1, cells are will exert larger stresses than

cells cultured on soft gels. In the presence of contractile inhibitors, morphological and contractile differences seen between soft and stiff substrata are lessened significantly.

CHAPTER 4: DISCUSSION

In this study, we used a polyacrylamide gel system to study the effects of ECM stiffness on the myofibroblastic activation and contractility of cultured primary rabbit corneal keratocytes treated with TGF-β1. PAAM hydrogels were prepared as described previously and functionalized with type I collagen. The elastic modulus of the specific PAAM gel preparation used in this study was higher than those of the equivalent preparation reported by Tse and Engler[65]. One reason this may have occurred is because of the differences in how mechanical testing was performed. Our approach measures the macroscopic properties of the ECM by dynamically compressing the whole material. Whereas in this report, elastic modulus was determined using atomic force microscopy (AFM) which measures properties on much smaller length scales and it is not always clear if this method will provide the same values. DMA tests showed that the PAAM gels being fabricated were 1.16 ± 0.25 kPa (soft) and 11.21 ± 0.67 kPa (stiff). These values corresponded well with measurements of corneal tissue before injury[10].

NRKs cultured on stiff (10 kPa) hydrogels glass coverslips in the presence of exogenous TGF-β1 exhibited broad morphologies along with an abundance of stress fibers. Whereas on soft (1 kPa) PAAM gels, keratocytes formed long, thin protrusions from the cell body and very few stress fibers were observed. The phenotype witnessed on the soft PAAM gels seemed to be more indicative of a quiescent keratocyte. Quantified cell area, length, and aspect ratio validated what was observed qualitatively. With respect to cell area, as the stiffness transitioned from glass to soft, a significant decrease was observed. Similarly, when evaluating end-to-end cell lengths, a decrease was observed for cells cultured on compliant substrata. Lastly, the opposite trend was noticed when analyzing cell aspect ratio, with cells becoming increasingly more elongated when

plated on soft substrates. By utilizing a serum-free culture method developed by Jester and colleagues to maintain a quiescent phenotype in the cultured NRKs[73], we observed similar morphologies to those reported by the Jester et al when cells were cultured on collagen-coated glass coverslips in either serum-free or TGF-beta treatment conditions[74]. In the current study, however, we also observed these morphologies on stiff PA gels, which helps validate our use of the PA gel system.

Additionally, other investigators have used a similar PAAM gel-based system to study the effects of ECM stiffness on the activation of other fibroblastic cell types, including dermal fibroblasts[75], and valvular interstitial cells[76]. Specifically, Dreier and colleagues used a similar PAAM gel system to show that qPCR measurements of α-SMA mRNA expression is modulated in human keratocytes cultured on gels of different stiffness[77]. As stiffness of the PAAM gels increased, the authors reported a concomitant increase in α-SMA mRNA expression levels. In the current study, however, we quantified the fraction of cells with positive staining for α-SMA immunofluorescence. Similar to the Dreier study, we also observed how ECM stiffness regulates the activation of rabbit corneal keratocytes via immunofluorescent staining of α-SMA. As PAAM gel stiffness increased, so did the fraction of α-SMA positive keratocytes. However, when plated on a 1 kPa PAAM substrate, the fraction dropped significantly, nearly to serum free levels. It is important to note that the Dreier study used keratocytes from a human subject whereas we used rabbit keratocytes. As mentioned earlier, human stromal tissue has a significantly higher elastic modulus than that of rabbits. In their results they observed less activation of keratocytes on 10 kPa substrates than on tissue culture plastic, whereas we see similar amounts of activation of NRKs on

stiff PAAM gels and glass coverslips. These results suggests a species dependent factor causing difference between our results.

Moreover, the current study identifies a similar stiffness-dependent modulation of myofibroblastic activation, but also investigates the spatiotemporal effects of cytoskeletal contractility on this process. To better understand how stiffness regulates cytoskeletal contractility, phopho-myosin light chains were stained in order to determine where contractions were occurring within the cell. On stiff substrates and glass coverslips, pMLC immunofluorescence appeared along the stress fibers of the cell, homogenously distributed throughout the cell. On the contrary, when plated on soft substrates pMLC was isolated to the distal tips of cell extensions. These differences in contractility likely influence the distribution and dynamics of focal adhesion inside the cells, which remains unclear. As discussed previously, pMLC plays an important role in the activation of the Rho pathway[26,39,40] which signals for the formation of stress fibers and focal adhesions. On stiffer gels, cells are able to exert higher contractile forces those on softer gels. One hypothesis explains these results. Through this process, mature focal adhesions are able to form and FAK pathways begin to activates Rho pathway. This motivates a feedback loop between pathways resulting in an increase in contractility on more rigid substrates. On soft substrates, mature focal adhesions may not form and FAK is not activated, and the cell does not transform into a myofibroblastic phenotype in the presence of TGF-β1. This hypothesis was further validated when contractile forces were quantified. On soft PAAM gels in the presence of TGF-β1, peak contractile stresses and net forces were significantly lower than those on stiffer substrates.

To further investigate the role of contractility in the activation of corneal keratocytes, blebbistatin was used to inhibit non-muscle myosin II, and consequentially contractility. By

disrupting contractility of NRKs in the presence of TGF-β1, stiffness-dependent variances in morphologies were significantly reduced. On stiff gels and glass substrates, cells appeared more dendritic and stress fibers were no longer present. Similar works by the Murphy lab explored how disrupting cell cytoskeletal structure using Latrunculin B (Lat-B) impacted the activation of corneal keratocytes[78]. Lat-B will effectively knock out cell contractility by binding to monomeric G-actin and preventing actin polymerization. Changes in myofibroblastic transformation of rabbit corneal fibroblasts were quantified by both analyzing mRNA expression using qPCR and calculating the fraction of cells fluorescently stained for α-SMA in the presence of Latrunculin B. Results show that in the presence of Lat-B, levels of α-SMA decreased significantly compared to those cultured in DMSO[78]. It would be interesting to further investigate the role of contractility by analyzing the fraction of α-SMA positive cells in the presence of TGF-β1 and blebbistatin.

Along with TGF-β1, many other growth factors and cytokines enter the stromal layer from the epithelium during injury. PDGF-BB[25], FGF-2[19,26] and EGF[19], all play a role in activating keratocytes and inducing a change into a repair phenotype. Assuming that the mechanotrasnsductive pathways involved remains constant in the transformation of these cells, it would be interesting to see how modulating the stiffness modulates the effect of each of these growth factors. For instance, similar changes in ECM stiffness could modulate the levels of PDGF-BB-driven keratocyte proliferation and motility. In our work, stiffness plays a crucial rooe in the wound healing process within the cornea. Although, the mechanotranductive pathways that control these cell behaviors are not well understood, these data suggest that pathways involving cell contractility- Rho, Rac, FAK - are likely involved in this process. It would be interesting to advance these studies by identifying the upstream regulators that are controlling these pathways.

CHAPTER 5: CONCLUSIONS AND FUTURE WORKS

From these results, it is clear that ECM stiffness plays a key role in the activation of quiescent corneal keratocytes to a myofibroblasts state in response to TGF-β1. This decrease in activation on more compliant substrates is also accompanies a change in morphology and decrease in contractility. On more compliant substrates, the cells will spread less, elongate more and form fewer stress fibers. Also on softer substrates, TGF-β1-driven NRKs exerted substantially less traction forces than those on stiffer substrates. However, it is still unclear how stiffness effects the fibrotic response by these cells.

Along with TGF-β1, other growth factors play an important role in the restoration of the cornea after injury. PDGF-BB, in particular, has been shown to increase the proliferation and motility of the cell. Preliminary studies (Appendix B, Fig. B1) suggest that substratum stiffness may play a role modulating cellular morphologies of PDGF-BB-treated cells. Based on these results, subsequent changes in proliferation and motility could occur. Thus, further testing is needed to identify changes in PDGF-BB-driven NRKs. Such experiments can include analyzing proliferation by quantifying the fraction of positive EdU stained NRKs on each substrate or by measuring motility of the cell by tracking their movements via time-lapse imaging.

Furthermore, this study was performed on a 2D platform using monomeric collagen. Future works should stride to make a more physiologically accurate model by utilizing a 3D model and filamentous type I collagen. Initial studies in our lab have shown that by activating both dorsal and ventral receptors of human telomerase transcriptase corneal fibroblasts (HTK cells) using a pseudo-3D PAAM gel system (Appendix B, Fig. B2), cells exhibit more elongated morphologies than on 2D substrata. In future works, we hope to seed primary rabbit corneal keratocytes in this

3D environment to study the effects on activation through TGF-β1 or PDGF-BB. Additionally, the highly-aligned microstructure of the corneal stroma is a key property that must be considered in future models. Therefore, through utilization of microfluidic devices, we have shown that we can polymerize collagen fibers onto PAAM gels and seed HTK cells onto these aligned fibers (Appendix B Fig. B3). Again, NRK culture experiments can be performed to investigates the effects of growth factors on primary keratocytes when plated on aligned collagen fibers and flexible substrata.

Lastly, as discussed, several mechanotransductive pathways seem to play a role in modulating the activation and contractility of NRKs. However, further work is needed to pinpoint these regulator pathways. Specifically, immunofluorescence staining should be performed to observe changes in localization and presence of YAP/TAZ and pFAK when cells are plated on soft or stiff gels or glass coverslips in the presence or absence of TGF-β1. Moreover, results from this study can be further expanded upon by analyzing the relationship between cytoskeletal dynamics and ECM stiffness. For instance, TFM experiments coupled with SiR-actin (Appendix B, Fig. B5) labeling to observe actin dynamics within a cell while simultaneously quantifying the forces they are exerting.

This research has potential in aiding the development of therapies for wound healing after refractive surgery or general trauma to the cornea. Tissue engineers can utilize these data to better understand the importance in creating devices of similar mechanical stiffness to that of normal, healthy tissue. Also, by identifying a target mechaotransudctive pathway, therapeutic drugs could also be used or developed to inhibit a cells ability to transform into a myofibroblastic phenotype.

All of these could be used to better improve ocular properties of the cornea and prevent issue such as corneal hazing, fibrosis, and visual impairment.

APPENDIX A: PROTOCOLS

Glass Slide Treatments:

1. Incubate slides in 0.1 M NaOH for ~ 60 min:
    a. Create 0.1 M NaOH solution
    b. Drop slides into solution one-by-one
    c. Incubate in solution for ~1hr (look for change in surface chemistry)
    d. Remove slides and rinse with MQ water
        i. Fill three small beakers with MQ water and dip slides sequentially
    e. Blow dry completely using N2
    f. Store in desiccator

Steps 2 and 3 are for BOTTOM slides only:

2. Incubate slides in 2% APTMS diluted with acetone for 30 min.
    a. [In fume hood] prepare a fresh solution of APTMS by mixing 98 mL of acetone with 2 mL of APTMS (open and pipette APTMS in a N_2 filled bag) in a clean beaker
    b. Pipette up and down/swirl carefully to mix
    c. Add slides one by one using forceps
    d. Let the slides incubate in the solution for 30 minutes
    e. Remove the slides one-by-one and dip into a small beaker of fresh acetone
    f. Allow to air dry [Can be stored in desiccator after this step]
3. Incubate slides with 0.5% glutaraldehyde diluted with 1XPBS for 30 min
    a. [In fume hood] In a clean dry beaker, add 99 mL of 1XPBS and 1 mL of glutaraldehyde
    b. Pipette up and down/swirl the solution to mix
    c. Let sit for 30 min
    d. Transfer the slides to a beaker of 1XPBS
    e. Sequentially dip the slides into 1 beaker of PBS followed by 3 beakers of water
    f. Blow dry with N_2 and place in desiccator

Step 4 is for TOP slides only:

4. [In fume hood] incubate slides in 2% DCDMS diluted in toluene for 30 min.
    a. Make a fresh solution of DCDMS and toluene mixing 98 mL of toluene with 2 mL of DCDMS
    b. Place 0.1 M NaOH treated slides in the solution one by one.
    c. Allow to incubate for 30 min
    d. Take out slides and dip them into a beaker of methanol
    e. Allow to air dry and then place in desiccator for future use

Polyacrylamide Gel Fabrication

5. Choose a desired elastic modulus for your polyacrylamide gels. (Table 1 annd 2)
    a. First add dH2O to a 1.5 mL microcentrifuge tube, followed by the appropriate volumes of acrylamide and bis-acrylamide
    b. Place the tube in a desiccator for 30 min to degas
    c. Before removing the tube from the desiccator, mix a 10% solution of ammonium persulfate.
        i. 100 uL of MQ water and 10 mg of APS
    d. Add the appropriate volumes of TEMED and 10% APS to you microcentrifuge tube to initiate polymerization
    e. Vortex to ensure proper mixing (make sure there are no bubbles)
6. Pipette 40 µL of the polyacrylamide solution onto one of the bottom slides
    a. Hold the pipette perpendicular to the slide and touch the pipette to the slide to avoid loss
7. Carefully cover the polyacrylamide solution with a top slide
    a. Angle down slowly
    b. The top slide should slide into place once placed on the bottom slide
    c. Avoid bubbles and leaks
8. Let polymerize for 30 min in desiccator
    a. You can then use then immediately or store them in 1XPBS in the 4C refrigerator.
    b. Wrap dishes in Parafilm
    c. Gels will keep for at 4C for a few weeks

Table A1. Recipes for PAAM gels used in normal cell culture and their respective volumes of acrylamide, bis-acrylamide, water, APS and TEMED.

Elastic Modulus	H_2O	40% Acrylamide	2% Bis-Acrylamide	TEMED	APS
1,150 Pa	695 µL	75 µL	30 µL	0.5 µL	5 µL
11,200Pa	895 µL	125 µL	175 µL	0.5 µL	5 µL

Table A2. Recipes for PAAM gels used in TFM cell culture and their respective volumes of acrylamide, bis-acrylamide, water, APS, TEMED, and bead solution.

Elastic Modulus	H_2O	40% Acrylamide	2% Bis-Acrylamide	TEMED	APS	Bead Solution
1,150 Pa	595 µL	75 µL	30 µL	0.5 µL	5 µL	100 µL
11,200 Pa	795 µL	125 µL	175 µL	0.5 µL	5 µL	100 µL

Polyacrylamide Gel Functionalization

1. Transfer glass slides with gels in between to a separate petri dish filled with 1XPBS, keeping the gels right side up and as submerged as possible, sue tweezers to remove the top glass slide from the gel. Place the glass slide with the gel into another petri dish filled with 1XPBS
2. [In the Tissue Culture Hood] Aspirate the 1XPBS and move slides to a new untreated petri dish.
    a. Use sterilized tweezers that have been dipped in ethanol and allowed to air dry.
    b. To help get the slides off the bottom of the dish. Press Finger into the bottom of the dish to lift slides off.
3. Sterilize the gels by washing once with Ethanol (EtOH)
    a. Make sure gels are completely submerged in the EtOH
    b. Gels should turn white when in EtOH
4. Wash gels in sterile 1XPBS three times to remove excess EtOH
5. Wash gels once with 50 mM HEPES (pH 8.5)
    a. Before aspirating off the HEPES, allow to sit while preparing the sulfo-SANPAH solution.
6. **Sulfo-SANPAH solution prep:**
    a. Using a 15mL falcon tube, mix a 1 mg/ml solution of sulfo-SANPAH in DI H_2O.
    b. Wrap in foil for long term use.
    c. Each gel will require 220µL of solution per treatment.
        i. Ex. For 8 slides and two treatments you will need 4 mg sulfo-SANPAH in 4mL DI H_2O.
7. Aspirate HEPES. Move slide to new untreated petri dishes and add 220µL of sulfo-SANPAH solution to each gel. Spread the solution by gently swirling or using a pipette tip to guide the solution across the gel until it is completely covered.
8. Treat gels under UV light for 10 minutes. Get gels as close to the light as possible.
9. Wash gels with HEPES. Repeat steps 7-8.
10. Wash gel three times with HEPES and then move to an untreated petri dish.

Preparation of Collagen Solution:

For one 6-well plate, make 20 mL of 50 µg/mL type I collagen by mixing in order the following:

1. 1.596 mL 10XMEM (Gibco #11430-030)
2. 0.04166 mL 0.1 N NaOH (make fresh every few months)
3. 18.029 mL DMEM (Sigma #D6046, with 1% Penicillin)
4. 0.333 mL Collagen (PurCol Bovine Collagen #5005)

Add 3 mL to each well of the plate and let incubate at 37°C for exactly 30 min. Then wash twice with DMEM and replace with sterile PBS at the end. Gels are now ready for cell culture

APPENDIX B: SUPPLEMENTARY EXPERIMENTAL RESULTS

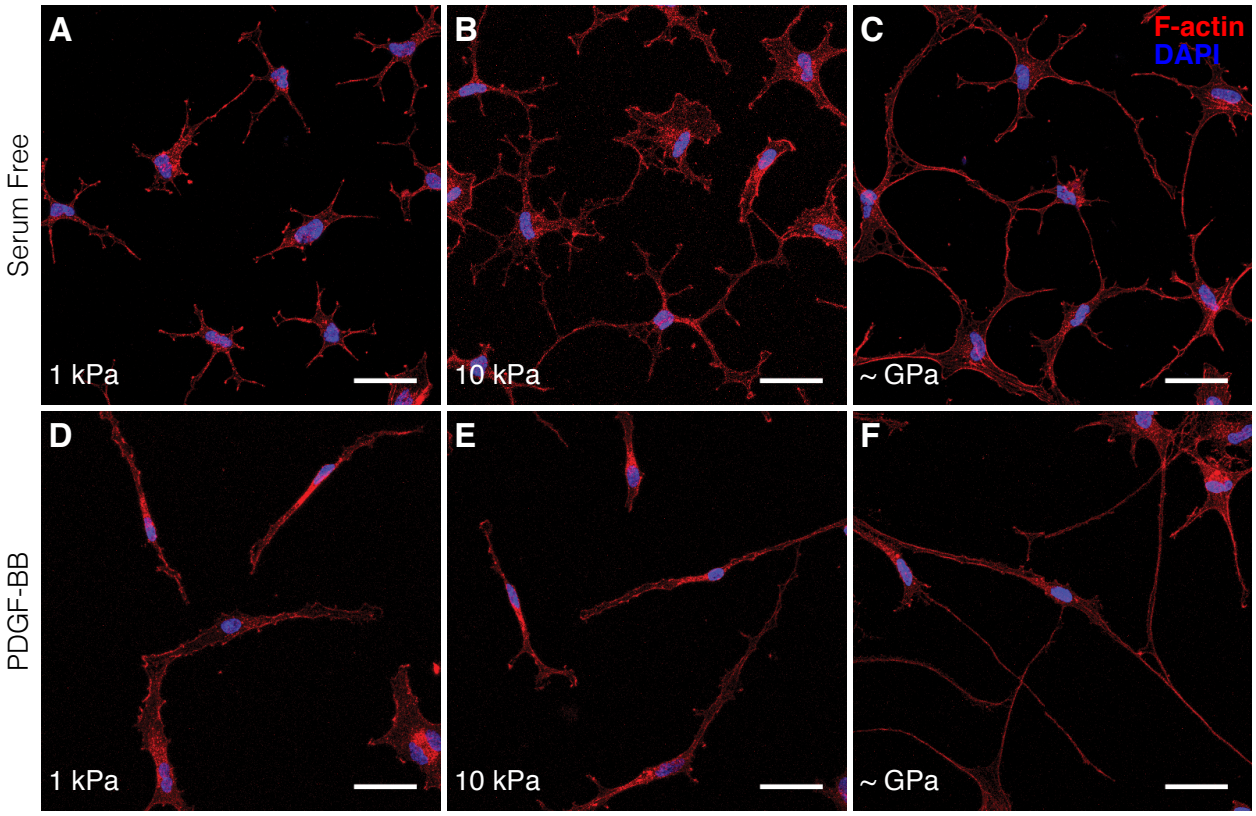

Figure B1. (A-F) Characteristic confocal fluorescence images of fixed corneal keratocytes cultured on either 1 kPa (A and D) or 10 kPa (B and E) polyacrylamide gels, or glass (C and F) coverslips, functionalized with type I collagen monomers. Prior to fixation, cells were cultured in either serum free media (A-C) or media containing PDGF-BB (D-F) for 5 days. Keratocytes were stained using phalloidin (red) and DAPI (blue) to visualize F-actin and nuclei, respectively. Scale bars are 50 μm. On glass substrates, PDGF-BB-driven NRKs exhibited very long and thin processes, and appeared very elongated. However, when cultured on either soft or stiff PAAM gel, the NRKs were less elongated and the processes were broader.

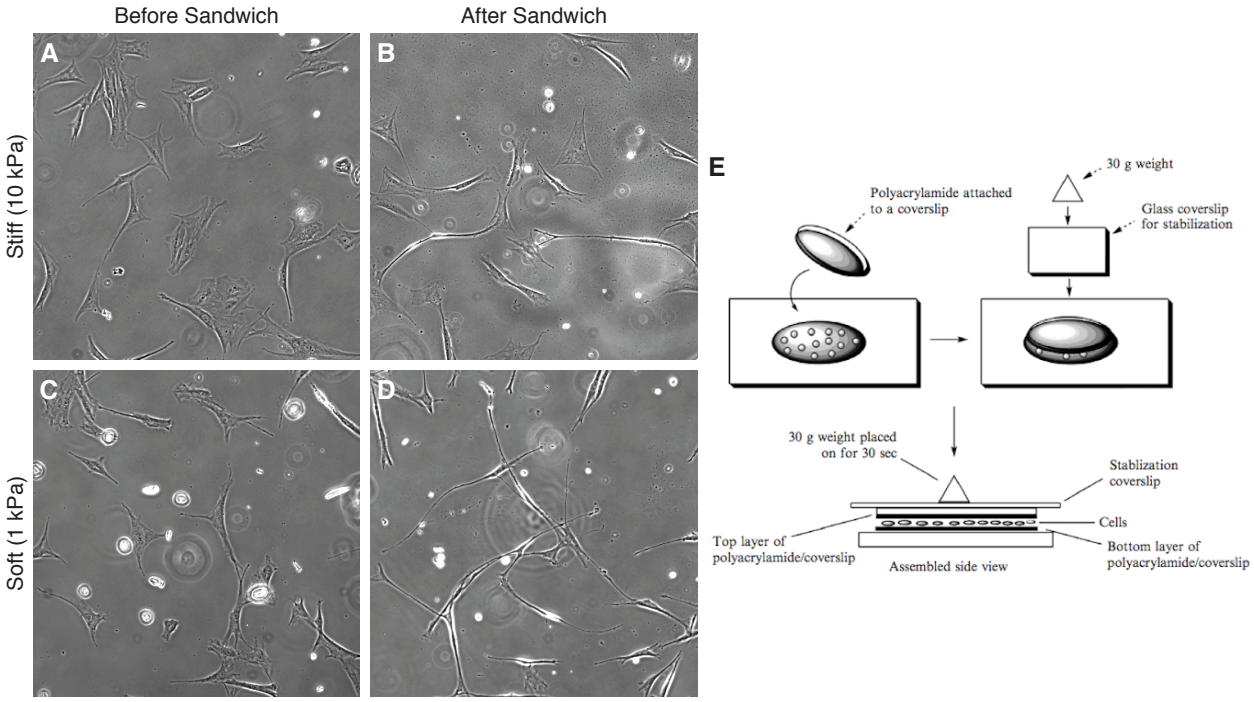

Figure B2. (A-D) Characteristic phase images of cultured human telomerase transcriptase corneal fibroblasts cells on soft (C-D) or stiff (A-B) polyacrylamide gels functionalized with type I monomeric collagen in 10% FBS containing media. Cells were first plated for 24 hours on a 2-dimensional platform (A and C), after 24 hours, another functionalized polyacrylamide gel was placed on top of the cells to create a pseudo 3-dimensional environment (B and D). (E) Schematic and protocols, obtained from Beningo et al[73], used to perform the 3D culture.

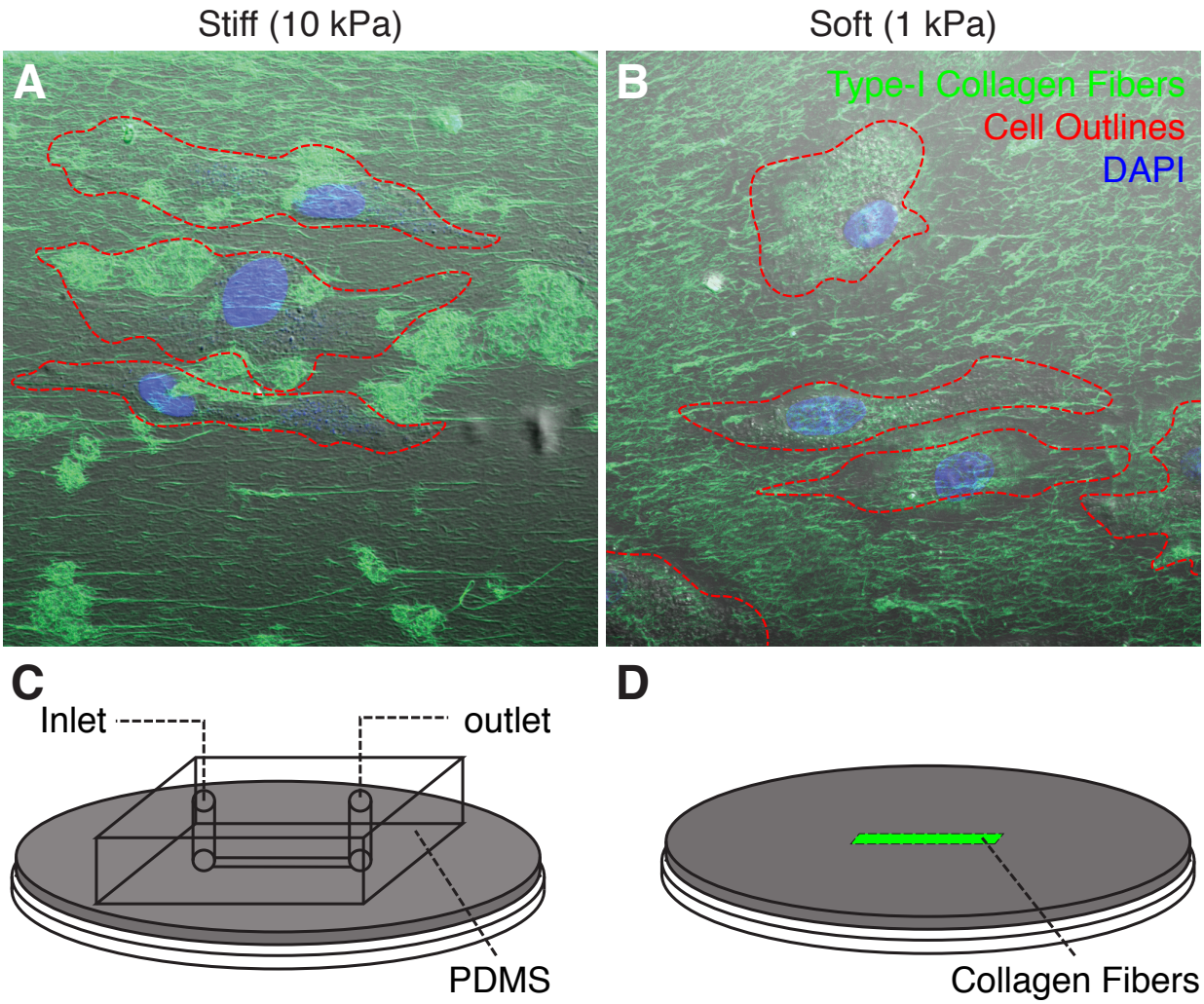

Figure B3. (A and C) Confocal DIC and fluorescent images of DAPI (blue) stained HTK cells (dashed red line) on type I collagen fibers (green) on either soft (C) or stiff (A) polyacrylamide gels. (C and D) Schematic images of how fibrous collagen was conjugated on PAAM gels. (C) A PDMS microfluidic channel was attached to the PAAM and PurCol collagen was infused through the 1500 μm × 50 μm × 15mm channel where it would polymerize to form fibers. (D) A stripe of aligned collagen fibers was deposited on the PAAM surface and stained with DTAF (green) for visualization. Cells attached and aligned in the direction of the collagen fibers. Future works will aim to optimize this protocol, study the effects of fiber alignment on cell traction forces, and investigate how fiber alignment regulates other cell phenotypes.

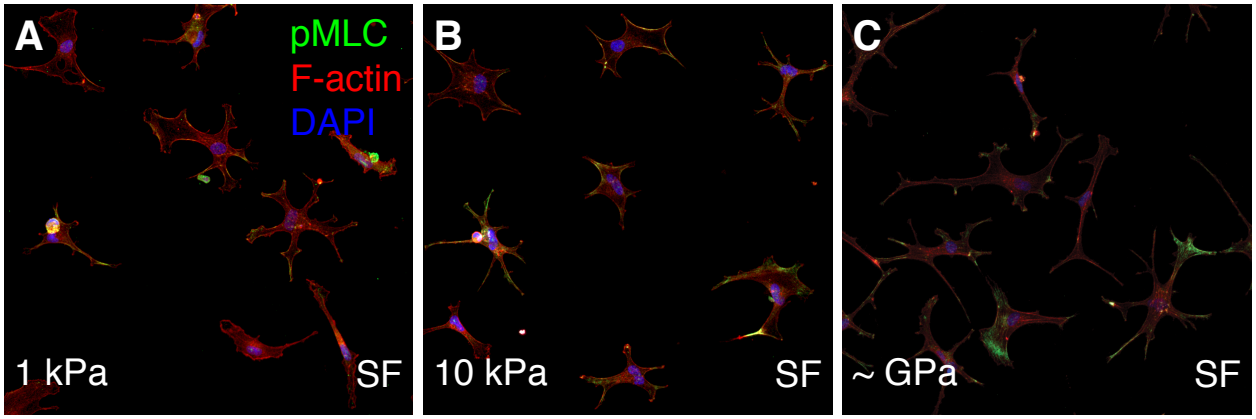

Figure B4. (A-C) Characteristic confocal fluorescence images of fixed corneal keratocytes cultured on either 1 kPa (A) or 10 kPa (B) polyacrylamide gels, or glass (C) coverslips, functionalized with type I collagen monomers. Prior to fixation, cells were cultured in either serum free media for 5 days. Keratocytes were stained using phalloidin (red), DAPI (blue), and pMLC immunofluorescence (green) to visualize F-actin, nuclei, and pMLC, respectively.

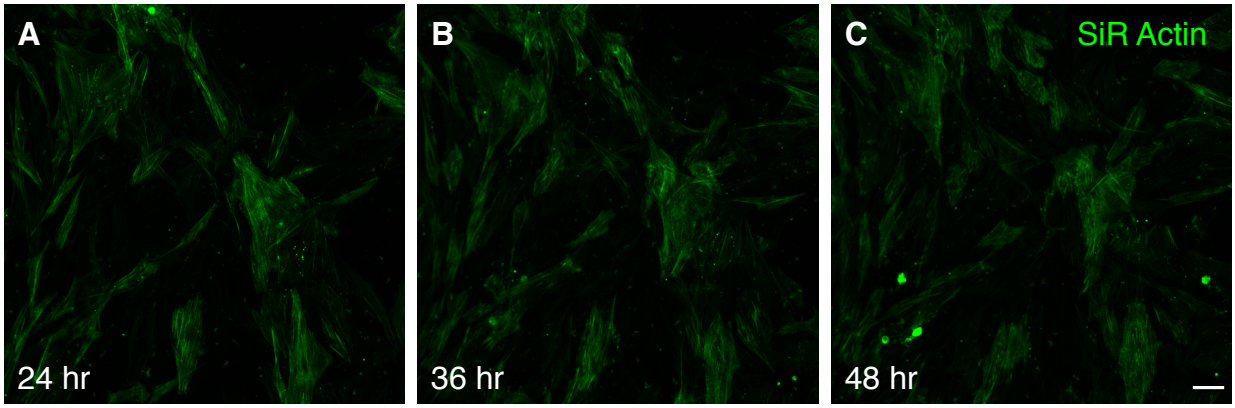

Figure B5. (A-C) Characteristic confocal fluorescent images of HTK cells on glass coverslips over a 24-hour span with images being captured every 20 min. Cell cytoskeletal structures were labeled using an SiR actin kit (CY-SC001; Cytoskeleton, Denver, CO) which was supplemented into the cell media at a ratio of 1:10,000 (SiR:Media). Over the 24 hour time-lapse, cell labeling remained robust.

REFERENCES

1. Alio, J. L., & Azar, D. T. (2018). *Management of Complications in Refractive Surgery*. Cham: Springer International Publishing.

2. Myopia (Nearsightedness). (2018). Retrieved from https://www.aoa.org/patients-and-public/eye-and-vision-problems/glossary-of-eye-and-vision-conditions/myopia.

3. Vitale, S. (2009). Increased Prevalence of Myopia in the United States Between 1971-1972 and 1999-2004. *Archives of Ophthalmology,127*(12), 1632.

4. Polak, L. (2013). Helping patients make the right decisions about treatment. *BMJ,347*(Oct09 4).

5. Taneri, S., Zieske, J., & Azar, D. (2004). Evolution, techniques, clinical outcomes, and pathophysiology of LASEK: Review of the literature. *Survey of Ophthalmology,49*(6), 576-602.

6. Wilson, S. E. (2004). Use of Lasers for Vision Correction of Nearsightedness and Farsightedness. *New England Journal of Medicine,351*(5), 470-475.

7. Meek, K. (2009). Corneal collagen—its role in maintaining corneal shape and transparency. *Biophysical Reviews*, *1*(2), 83-93.

8. Torricelli, A., Singh, V., Santhiago, M., & Wilson, S. (2013). The Corneal Epithelial Basement Membrane: Structure, Function, and Disease. *Investigative Opthalmology & Visual Science*, *54*(9), 6390.

9. Facts About the Cornea and Corneal Disease | National Eye Institute. (2018). Retrieved from *https://nei.nih.gov/health/cornealdisease.*

10. Thomasy, S., Raghunathan, V., Winkler, M., Reilly, C., Sadeli, A., & Russell, P. et al. (2014). Elastic modulus and collagen organization of the rabbit cornea: Epithelium to endothelium. *Acta Biomaterialia*, *10*(2), 785-791.

11. SMILE, LASIK or PRK: Which is Best? - LaserVue Eye Center. (2018). Retrieved from *https://www.laservue.com/smile/smile-lasik-or-prk-which-is-best/.*

12. Hayes S, Boote C, Lewis J *et al*. Comparative study of fibrillar collagen arrangement in the corneas of primates and other mammals. *Anat Rec* 2007; **290**: 1542–1550.

13. Meek KM & Boote C. The use of X-ray scattering techniques to quantify the orientation and distribution of collagen in the corneal stroma. *Prog Retin Eye Res* 2009; **28**: 369–392.

14. Dua, H. S., & Azuara-Blanco, A. (2000). Limbal stem cells of the corneal epithelium. *Survey of Ophthalmology, 44*(5), 415–425.

15. Dua, H. S., Shanmuganathan, V. A., Powell-Richards, A. O., Tighe, P. J., & Joseph, A. (2005). Limbal epithelial crypts: A novel anatomical structure and a putative limbal stem cell niche. *The British Journal of Ophthalmology, 89*(5), 529–532.

16. Funderburgh JL, Mann MM, Funderburgh ML. Keratocyte phenotype mediates proteoglycan structure: a role for fibroblasts in corneal fibrosis. *J Biol Chem*. 2003;278:45629–45637.

17. Hassell JR, Birk DE. The molecular basis of corneal transparency. *Exp Eye Res*. 2010;91:326–335.

18. Plotnikov, S. V., Sabass, B., Schwarz, U. S., & Waterman, C. M. (2014). High-resolution traction force microscopy. *Methods in cell biology*, *123*, 367-94.

19. Wilson, S., Schultz, G., Chegini, N., Weng, J., & He, Y. (1994). Epidermal Growth Factor, Transforming Growth Factor Alpha, Transforming Growth Factor Beta, Acidic Fibroblast Growth Factor, Basic Fibroblast Growth Factor, and Interleukin-1 Proteins in the Cornea. *Experimental Eye Research*, *59*(1), 63-72.

20. Wilson, S., He, Y., Weng, J., Li, Q., Mcdowall, A., Vital, M., & Chwang, E. (1996). Epithelial Injury Induces Keratocyte Apoptosis: Hypothesized Role for the Interleukin-1 System in the Modulation of Corneal Tissue Organization and Wound Healing. *Experimental Eye Research*, *62*(4), 325-338.

21. Jester JV, Huang J, Barry-Lane PA, Kao WW, Petroll WM, Cavanagh HD. Transforming growth factorbeta)-mediated corneal myofibroblast differentiation requires actin and fibronectin assembly. *Invest Ophthalmol Vis Sci*. 1999a;40:1959–1967.

22. Farjo A, McDermott M, Soong HK. Corneal anatomy, physiology, and wound healing. In: Yanoff M, Duker JS, eds, *Ophthalmology*, 3rd ed. St. Louis, MO, Mosby, 2008; 203–208

23. Fini, M. E., & Stramer, B. M. (2005). How the cornea heals: cornea- specific repair mechanisms affecting surgical outcomes. *Cornea*, *24*(8 Suppl 1), S2–S11.

24. Geroski DH, Matsuda M, Yee RW, Edelhauser HF. Pump function of the human corneal endothelium; effects of age and cornea guttata. *Ophthalmology* 1985; 92:759–763; discussion by J Sugar, 763.

25. Zhou C. The Functional Roles of Rho-kinase and Matrix Metalloproteinases in Regulating Corneal Stromal Cell Mechanics in 3-D Collagen Matrices, Biomedical Engineering Program. University of Texas Southwestern Medical Center; 2014.

26. Chen J, Guerriero E, Sado Y, SundarRaj N. Rho-mediated regulation of TGF-beta1- and FGF-2-induced activation of corneal stromal keratocytes. *Invest Ophthalmol Vis Sci*. 2009;50:3662–3670.

27. Lakshman N, Petroll WM. Growth factor regulation of corneal keratocyte mechanical phenotypes in 3-D collagen matrices. Invest Ophthalmol Vis Sci. 2012;53:1077–1086.

28. Kim A, Zhou C, Lakshman N, Petroll WM. Corneal Stromal Cells use both Highand Low-Contractility Migration Mechanisms in 3-D Collagen Matrices. *Exp Cell Res*. 2012a;318:741–752.

29. Blalock TD, Duncan MR, Varela JC, Goldstein MH, Tuli MH, Grotensdorst GR, Schultz GS. Connective tissue growth factor expression and action in human corneal fibroblast cultures and rat corneas after photorefractive keratectomy. *Invest Ophthalmol Vis Sci*. 2003;44:1879–1887.

30. Karamichos D, Guo XQ, Hutcheon AE, Zieske JD. Human corneal fibrosis: an in vitro model. Invest Ophthalmol Vis Sci. 2010;51:1382–1388.

31. Moller-Pedersen T, Cavanagh HD, Petroll WM, Jester JV. Stromal wound healing explains refractive instability and haze development after photorefractive keratectomy: A 1-year confocal microscopic study. *Ophthalmology*. 2000; 107:1235–1245.

32. Boote C, Du Y, Morgan S, Harris J, Kamma-Lorger C, Hayes S, Lathrop K, Rob D, Burrow M, Hiller J, Terrill N, Funderburgh J, Meek K. Quantitative assessment of ultrastructure and light scatter in mouse corneal debridement wounds. *Invest Ophthalmol Vis Sci*. 2012;53:2786–2795.

33. Jester JV, Brown D, Pappa A, Vasilou V. Myofibroblast differentiation modulates keratocyte crystallin protein expression, concentration,, and cellular light scattering. *Invest Ophthalmol Vis Sci*.2012;53:770–778.

34. Moller-Pedersen T, Cavanagh HD, Petroll WM, Jester JV. Corneal haze development after PRK is regulated by volume of stromal tissue removal. *Cornea*. 1998a;17:627–639.

35. Moller-Pedersen T, Cavanagh HD, Petroll WM, Jester JV. Stromal wound healing explains refractive instability and haze development after photorefractive keratectomy: A 1-year confocal microscopic study. *Ophthalmology*. 2000;107:1235–1245.

36. Ljubimov, A., & Saghizadeh, M. (2015). Progress in corneal wound healing. *Progress In Retinal And Eye Research*, *49*, 17-45.

37. Thomasy, S., Raghunathan, V., Winkler, M., Reilly, C., Sadeli, A., & Russell, P. et al. (2014). Elastic modulus and collagen organization of the rabbit cornea: Epithelium to endothelium. *Acta Biomaterialia*, *10*(2), 785-791.

38. Achterberg, V., Buscemi, L., Diekmann, H., Smith-Clerc, J., Schwengler, H., & Meister, J. et al. (2014). The Nano-Scale Mechanical Properties of the Extracellular Matrix Regulate Dermal Fibroblast Function. *Journal Of Investigative Dermatology*, *134*(7), 1862-1872.

39. Anderson S, DiCesare L, Tan I, Leung T, SundarRaj N. Rho-mediated assembly of stress fibers is differentially regulated in corneal fibroblats and myofibroblasts. *Exp Cell Res*. 2004;298:574–583.

40. Amano M, Chihara K, Nakamura N, Fukata Y, Yano T, Shibata M, Ikebe M, Kaibuchi K. Myosin II activation promotes neurite retraction during the action of Rho and Rho-kinase. *Genes Cells*.1998;3:177–188.

41. Svitkina TM, Borisy GG. Arp2/3 complex and actin depolymerizing factor/cofilin in dendritic organization and treadmilling of actin filament array in lamellipodia. *J Cell Biol*. 1999;145:1009–1026.

42. emali KA, Burridge K. Coupling membrane protrusion and cell adhesion. *J Cell Sci.*2003;116:2389–2397.

43. Piccolo S, Dupont S, Cordenonsi M. The biology of YAP/TAZ: hippo signaling and beyond. Physiol Rev2014;94:1287-312. 10.1152/physrev.00005.2014.

44. Vassilev, A. (2001). TEAD/TEF transcription factors utilize the activation domain of YAP65, a Src/Yes-associated protein localized in the cytoplasm. *Genes & Development*, *15*(10), 1229-1241.

45. Zhao, B. *et al.* Inactivation of YAP oncoprotein by the Hippo pathway is involved in cell contact inhibition and tissue growth control. *Genes Dev.* **21**, 2747–2761 (2007).

46. Mohri, Z., Del Rio Hernandez, A., & Krams, R. (2017). The emerging role of YAP/TAZ in mechanotransduction. *Journal Of Thoracic Disease*, *9*(5), E507-E509.

47. Geiger, B., Spatz, J., & Bershadsky, A. (2009). Environmental sensing through focal adhesions. *Nature Reviews Molecular Cell Biology*, *10*(1), 21-33.

48. O'Brart DP, Patsoura E, Jaycock P, Rajan M, Marshall J. Excimer laser photorefractive keratectomy for hyperopia: 7.5-year follow-up. *J Cataract Refract Surg*. 2005;31:1104–13.

49. Gimbel, H., Anderson Penno, E., van Westenbrugge, J., Ferensowicz, M., & Furlong, M. (1998). Incidence and management of intraoperative and early postoperative complications in 1000 consecutive laser in situ keratomileusis cases. *Ophthalmology*, *105*(10), 1839-1848.

50. Reinstein, D., Archer, T., & Gobbe, M. (2014). Small incision lenticule extraction (SMILE) history, fundamentals of a new refractive surgery technique and clinical outcomes. *Eye And Vision*, *1*(1).

51. Wells R. G. (2013). Tissue mechanics and fibrosis. *Biochimica et biophysica acta*, *1832*(7), 884-90.

52. Wells, R. (2008). The role of matrix stiffness in regulating cell behavior. *Hepatology*, *47*(4), 1394-1400.

53. Sun, Z., Guo, S., & Fässler, R. (2016). Integrin-mediated mechanotransduction. *The Journal Of Cell Biology*, *215*(4), 445-456.

54. Yim EK and Sheetz MP (2012) Force-dependent cell signaling in stem cell differentiation. Stem Cell Research Therapy 3: 41.

55. Dingal, P.C., A.M. Bradshaw, S. Cho, M. Raab, A. Buxboim, J. Swift, and D.E.Discher. 2015. Fractal heterogeneity in minimal matrix models of scars modulates stiff-niche stem-cell responses via nuclear exit of a mechanorepressor. *Nat. Mater*.

56. Castillo AB, Blundo JT, Chen JC, Lee KL, YereddiNR, Jang E, Kumar S, Tang WJ, Zarrin S, Kim JB,et al. (2012) Focal adhesion kinase plays a role inosteoblast mechanotransduction in vitro but does notaffect load-induced bone formation in vivo. *PLoS One*7:e43291.

57. Dupont, S., Morsut, L., Aragona, M., Enzo, E., Giulitti, S., & Cordenonsi, M. et al. (2011). Role of YAP/TAZ in mechanotransduction. *Nature*, *474*(7350), 179-183.

58. Engler, A. J., Sen, S., Sweeney, H. L. & Discher, D. E. Matrix elasticity directs stem cell lineage specification. *Cell* 126, 677–689 (2006).

59. McBeath, R., Pirone, D. M., Nelson, C. M., Bhadriraju, K. & Chen, C. S. Cell shape, cytoskeletal tension, and RhoA regulate stem cell lineage commitment. *Dev. Cell* 6, 483–495 (2004).

60. Ren XD, Kiosses WB, Sieg DJ, Otey CA, Schlaepfer DD and Schwartz MA: Focal adhesion kinase suppresses Rho activity to promote focal adhesion turnover. *J Cell Sci*. 113:3673–3678. 2000.

61. Hsia, D., Mitra, S., Hauck, C., Streblow, D., Nelson, J., & Ilic, D. et al. (2003). Differential regulation of cell motility and invasion by FAK. *The Journal Of Cell Biology*, *160*(5), 753-767.

62. Katsumi, A., Orr, A., Tzima, E., & Schwartz, M. (2004). Integrins in Mechanotransduction. *Journal Of Biological Chemistry*, *279*(13), 12001-12004.

63. Wichterle, O., & Lím, D. (1960). Hydrophilic Gels for Biological Use. *Nature*, *185*(4706), 117-118.

64. Pelham, R., & Wang, Y. (1997). Cell locomotion and focal adhesions are regulated by substrate flexibility. *Proceedings Of The National Academy Of Sciences*, *94*(25), 13661-13665.

65. Tse, J., & Engler, A. (2010). Preparation of Hydrogel Substrates with Tunable Mechanical Properties. *Current Protocols In Cell Biology*, *47*(1), 10.16.1-10.16.16.

66. Beningo, K., Dembo, M., & Wang, Y. (2004). Responses of fibroblasts to anchorage of dorsal extracellular matrix receptors. *Proceedings Of The National Academy Of Sciences*, *101*(52), 18024-18029.

67. Guo, P., Yuan, Y., & Chi, F. (2014). Biomimetic alginate/polyacrylamide porous scaffold supports human mesenchymal stem cell proliferation and chondrogenesis. *Materials Science And Engineering: C*, *42*, 622-628.

68. Issaq, H., & Veenstra, T. (2008). Two-dimensional polyacrylamide gel electrophoresis (2D-PAGE): advances and perspectives. *Biotechniques*, *44*(5), 697-700.

69. Harris, A., Wild, P., & Stopak, D. (1980). Silicone rubber substrata: a new wrinkle in the study of cell locomotion. *Science*, *208*(4440), 177-179.

70. Pelham, R., & Wang, Y. (1999). High Resolution Detection of Mechanical Forces Exerted by Locomoting Fibroblasts on the Substrate. *Molecular Biology Of The Cell*, *10*(4), 935-945.

71. Sabass, B., Gardel, M., Waterman, C., & Schwarz, U. (2008). High Resolution Traction Force Microscopy Based on Experimental and Computational Advances. *Biophysical Journal*, *94*(1), 207-220.

72. Petroll WM, Ma L, Jester JV. Direct correlation of collagen matrix deformation with focal adhesion dynamics in living corneal fibro- blasts. J Cell Sci. 2003;116:1481–1491.

73. Jester, JV, Barry-Lane, PA, Cavanagh, HD, Petroll, WM. (1996) Induction of alpha-smooth muscle actin expression and myofibroblast transformation in cultured corneal keratocytes *Cornea* 15,505-516.

74. Jester, J.V. & Huang, JY & Barry-Lane, P.A. & Kao, Winston & Petroll, Walter & Cavanagh, Harrison. (1999). Transforming growth factor(β)-mediated corneal myofibroblast differentiation requires actin and fibronectin assembly. *Investigative ophthalmology & visual science*. 40. 1959-67.

75. Achterberg, V., Buscemi, L., Diekmann, H., Smith-Clerc, J., Schwengler, H., & Meister, J. et al. (2014). The Nano-Scale Mechanical Properties of the Extracellular Matrix Regulate Dermal Fibroblast Function. *Journal Of Investigative Dermatology*, *134*(7), 1862-1872.

76. Ma, H., Killaars, A. R., DelRio, F. W., Yang, C., & Anseth, K. S. (2017). Myofibroblastic activation of valvular interstitial cells is modulated by spatial variations in matrix elasticity and its organization. *Biomaterials*, *131*, 131-144.

77. Dreier, B., Thomasy, S. M., Mendonsa, R., Raghunathan, V. K., Russell, P., & Murphy, C. J. (2013). Substratum compliance modulates corneal fibroblast to myofibroblast transformation. *Investigative ophthalmology & visual science*, *54*(8), 5901-7.

78. Thomasy, S., Raghunathan, V., Miyagi, H., Evashenk, A., Sermeno, J., & Tripp, G. et al. (2018). Latrunculin B and substratum stiffness regulate corneal fibroblast to myofibroblast transformation. *Experimental Eye Research*, *170*, 101-107.

79. Last, J., Thomasy, S., Croasdale, C., Russell, P., & Murphy, C. (2012). Compliance profile of the human cornea as measured by atomic force microscopy. *Micron*, *43*(12), 1293-1298.

80. Martiel, J.-L., Leal, A., Kurzawa, L., Balland, M., Wang, I., Vignaud, T., Tseng, Q. and Théry, M. (2015). Measurement of cell traction forces with ImageJ. *Methods Cell Biol.* 125, 269–287.

81. Etemad-Moghadam S, Khalili M, Tirgary F, Alaeddin M. Evaluation of myofibroblasts in oral epithelial dysplasia and squamous cell carcinoma. *J Oral Pathol.* 2009;38:625–43.

82. Velasquez, L., Sutherland, L., Liu, Z., Grinnell, F., Kamm, K., & Schneider, J. et al. (2013). Activation of MRTF-A-dependent gene expression with a small molecule promotes myofibroblast differentiation and wound healing. *Proceedings Of The National Academy Of Sciences*, *110*(42), 16850-16855.

BIOGRAPHICAL SKETCH

Daniel Maruri was born in Waco, Texas in 1993. After graduating from Westlake High School in Austin, Texas in 2012, Daniel entered Purdue University in West Lafayette, Indiana. During his junior and senior years at Purdue, Daniel worked in Dr. Taeyoon Kim's Molecular, Cellular, and Tissue (MCT) Biomechanics Laboratory where he assisted investigative research focused towards better understanding the mechanical properties of the cytoskeleton, cells, and tissues. He received his Bachelor of Science in Biomedical Engineering from Purdue in 2016. After graduation, he then began his graduate studies at the University of Texas at Dallas in the fall semester of 2016. In October of 2016, Daniel would enter into Dr. Victor Varner's research lab as a research assistant where he would investigate how ECM stiffness influences wound healing processes within the cornea. He received his Master of Science from the University of Texas at Dallas in 2019.

VITAE

DANIEL P. MARURI

EDUCATION

Bachelor of Science in Biomedical Engineering, Graduated May of 2016

WELDON SCHOOL OF BIOMEDICAL ENGINEERING, PURDUE UNIVERSITY – West Lafayette, IN

Cumulative GPA – 3.04

Master of Science in Biomedical Engineering, Completed January of 2019

THE UNIVERSITY OF TEXAS AT DALLAS – Richardson, TX

Cumulative GPA – 3.704

EXPERIENCE HIGHLIGHTS

THE UNIVERSITY OF TEXAS AT DALLAS – Richardson, TX

Master's Thesis Research, September 2016 to Present

The scope of my research was focused on how changes in mechanical stiffness of the extracellular matrix regulates the transformation of primary corneal keratocytes into a myofibroblastic phenotype during wound healing. This research has the potential to improve therapeutic medicine for patients that experience traumatic injury to the cornea or undergo refractive surgery (PRK, LASIK, SMILE). During my time as a research assistant at UTD, I have developed skills to lead experimental design processes, think critically to solve problems, and establish timeframes to have deliverables ready in an efficient manner.

- Strong collaboration with the UT Southwestern ophthalmology department throughout the entirety of my research
- Presented research at a BMES seminar in Phoenix and Atlanta– 2017 and 2018

WELDON SCHOOL OF BIOMEDICAL ENGINEERING AND RESEARCH (PURDUE) – West Lafayette, IN

Senior Design Project, January 2015 to December 2015

Undergraduate Research, May 2015 to May 2016

The scope of my work includes the structure and dynamics of living cells. By understanding the physical and mechanical characteristic of cells, processes such as morphogenesis, differentiation, and movements can be further understood. This research will help further studies geared toward tissue engineering, muscle regeneration, and cancer treatment.

- Published as a contributor in PLOS Computational Biology

ORTHO KINEMATICS – Austin, TX

Medical Imaging Intern and Interim Quality Manager, May to August 2014

Prioritized, planned, and managed quality processes for a provider of transitional spinal imaging of the cerebral and thoracic regions. Defined milestones, tracked progress, and prepared detailed documentation. Learned the internal quality system and obtained an understanding of current FDA

requirements for document management and control, labeling, safety, and technologies. Enforced standard operating procedures (SOPs) through documentation and continuous oversight.

- Drafted and submitted clear, concise corrective and preventative actions (CAPAs) for issues identified through audits, engineering change notices (ECNs), and customer complaints.

TEXAS ENGINEERING SOLUTIONS – Austin, TX
Mentorship Program, June to August 2012
Engineering Internship, January to May 2012

SKILLS AND ACHIEVMENTS

► **Achievements:**

- *Presidential Scholarship: Scholarship given by Purdue University for "high academic achievement, leadership and service in school and community".*
  - *Only 15% of attending Purdue students receive any sort of scholarship*
- *Attended the Biomedical Engineering Seminar (BMES) in Phoenix where I presented my research at a conference*

► **Skills:**

- *Computer/Coding Software – Matlab | Python | C+ | Microsoft programs | ImageJ (FIJI) | Adobe programs |Zen/Nikon software | Rstudio*
- *3-D Modeling Programs – SolidWorks | AutoCAD Civil 3D |Autodesk 3Ds max*
- *Lab Experience - Performed dissections | Cell extractions from corneas |Immunofluorescence staining | Cell passaging | Cell plating | Microfluidics | Hydrogel fabrication | Protein conjugation | Traction Force Microscopy | Strong presentation skills*
- *Microscopy - Immunofluorescence Staining | DIC Imaging | Phase Imaging | Confocal | Time lapse setup*